



HAL
open science

Mineral systems prospectivity modelling for gold and nickel in the Halls Creek Orogen, Western Australia

Fariba Kohanpour, Sandra Occhipinti, Mark Douglas Lindsay, Weronika Gorczyk, Fred Jourdan, Marc Poujol

► **To cite this version:**

Fariba Kohanpour, Sandra Occhipinti, Mark Douglas Lindsay, Weronika Gorczyk, Fred Jourdan, et al.. Mineral systems prospectivity modelling for gold and nickel in the Halls Creek Orogen, Western Australia. *Ore Geology Reviews*, 2020, 127, pp.103809. 10.1016/j.oregeorev.2020.103809 . insu-02958921

HAL Id: insu-02958921

<https://insu.hal.science/insu-02958921>

Submitted on 14 Oct 2020

HAL is a multi-disciplinary open access archive for the deposit and dissemination of scientific research documents, whether they are published or not. The documents may come from teaching and research institutions in France or abroad, or from public or private research centers.

L'archive ouverte pluridisciplinaire **HAL**, est destinée au dépôt et à la diffusion de documents scientifiques de niveau recherche, publiés ou non, émanant des établissements d'enseignement et de recherche français ou étrangers, des laboratoires publics ou privés.

Journal Pre-proofs

Mineral systems prospectivity modelling for gold and nickel in the Halls Creek Orogen, Western Australia

Fariba Kohanpour, Sandra Occhipinti, Mark Lindsay, Weronika Gorczyk, Fred Jourdan, Marc Poujol

PII: S0169-1368(20)30629-6
DOI: <https://doi.org/10.1016/j.oregeorev.2020.103809>
Reference: OREGEO 103809

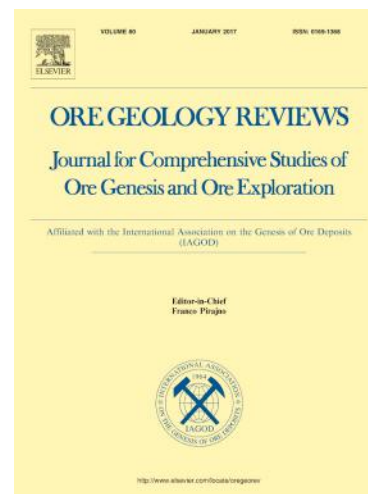
To appear in: *Ore Geology Reviews*

Received Date: 12 June 2020
Revised Date: 24 September 2020
Accepted Date: 28 September 2020

Please cite this article as: F. Kohanpour, S. Occhipinti, M. Lindsay, W. Gorczyk, F. Jourdan, M. Poujol, Mineral systems prospectivity modelling for gold and nickel in the Halls Creek Orogen, Western Australia, *Ore Geology Reviews* (2020), doi: <https://doi.org/10.1016/j.oregeorev.2020.103809>

This is a PDF file of an article that has undergone enhancements after acceptance, such as the addition of a cover page and metadata, and formatting for readability, but it is not yet the definitive version of record. This version will undergo additional copyediting, typesetting and review before it is published in its final form, but we are providing this version to give early visibility of the article. Please note that, during the production process, errors may be discovered which could affect the content, and all legal disclaimers that apply to the journal pertain.

© 2020 Published by Elsevier B.V.



Mineral systems prospectivity modelling for gold and nickel in the Halls Creek Orogen, Western Australia

Fariba Kohanpour^{a*}, Sandra Occhipinti^{a,b}, Mark Lindsay^a, Weronika Gorczyk^a, Fred Jourdan^c, Marc Poujol^d

^a Centre for Exploration Targeting, School of Earth Science, The University of Western Australia, 35 Stirling Highway, Crawley, WA 6009, Australia.

^b Commonwealth Scientific and Industrial Research Organisation (CSIRO) Mineral Resources, 26 Dick Perry Avenue, Kensington, WA 6151, Australia.

^c Western Australian Argon Isotope Facility, JdL Centre & School of Earth and Planetary Sciences, Curtin University, GPO Box U1987, Perth WA 6845, Australia.

^d Géosciences Rennes, UMR CNRS 6118, Université Rennes 1, F-35042 Rennes Cedex, France.

*Corresponding author: fariba.kohanpour@uwa.edu.au

Abstract

Geodynamic models, geological-geophysical interpretations, and isotope analysis illustrate that there are links between the nickel and gold mineral systems in the Halls Creek Orogen, Western Australia. Whole-rock Nd and $^{40}\text{Ar}/^{39}\text{Ar}$ analysis of rocks throughout the region, when compared with the geodynamic models suggest that nickel and gold mineralization in the Halls Creek Orogen can be related to basin development and subsequent basin closure during the convergence of North Australian Craton and Kimberley Craton, respectively. Whole-rock Nd analysis confirmed the input of juvenile melts in the centre of the orogen before the 1835–1805 Ma Halls Creek Orogeny, supporting the upwelling of decompression mantle melts during the basin development. These analyses also revealed the spatial links between nickel and gold mineralization and lithological units with positive ϵNd values. Spatially the link between these mineral systems appears to be related to the presence of deep-seated shear zones that formed early in the history of the orogen and were later reactivated. The results of geodynamic models, geophysical interpretation, and isotopic

analysis are used to understand the critical processes in the gold and nickel mineralization, which are presented by predictor maps. The GIS-based knowledge-driven fuzzy logic method used to integrate the predictor maps and create the prospectivity maps. Herein we show that mafic-ultramafic units prospective for nickel mineralization formed by upwelling of decompression mantle melt during crustal thinning and extension during basin development, and typically consist of the most juvenile magmas in the region. Whereas, gold deposits formed during the compressional regime and basin closure, and are located along a major shear zone separating two terranes. This deep crustal-scale shear zone is implied to be the site of multiple stages of deformation that acted as fluid migration pathways during basin closure and subsequent collision. Another critical element that appears to be related to gold prospectivity is the presence of lithologies with a juvenile signature. In contrast to nickel analyses which are closely related to mafic-ultramafic units, the source component seems less influential when attempting to target orogenic gold deposits.

Keywords: Mineral systems, Nd isotopic map, GIS prospectivity, age of gold mineralisation, Halls Creek Orogen.

1. Introduction

The mineral system concept emerged two decades ago as a targeting tool for mineral exploration (Wyborn et al., 1994). Mineral system analysis focusses on the critical geological processes that control the generation and preservation of mineral deposits (Blewett et al., 2010; Knox-Robinson and Wyborn, 1997; McCuaig et al., 2010; McCuaig and Hronsky, 2014; Occhipinti et al., 2016; Wyborn et al., 1994). Prospectivity mapping has arisen from mineral systems analysis (Dulfer et al., 2016; Joly et al., 2014; Joly et al., 2012; Lindsay et al., 2016a; Occhipinti et al., 2016) as a

result of increased availability of large-scale geophysical datasets, and a greater understanding of the Earth evolution and geodynamics (McCuaig and Hronsky, 2014), and advances in geographical information system (GIS) technologies.

The purpose of this paper is to identify and review the mineral system components of orthomagmatic nickel sulfide and orogenic gold mineralization in the Halls Creek Orogen and applying them in prospectivity modelling. The mineral system framework applied by Occhipinti et al. (2016), presented the practical critical elements including the lithospheric architecture, geodynamic throttle, fertility, depositional site, and preservation required for ore formation and preservation. In order to complete exploration targeting, the proxies for the mineral system parameters can be mapped from geoscience datasets, which then are statistically examined by GIS-based analysis (Bonham-Carter, 1994; Carranza, 2008; Kreuzer et al., 2010; Porwal and Carranza, 2015; Porwal et al., 2003). This allows prioritization of critical components for prospectivity analysis at a variety of scales (McCuaig et al., 2010). The results include a series of predictor maps for each mineral system component which are combined to estimate overall mineral potential across a region (Joly et al., 2014; Occhipinti et al., 2016).

The Halls Creek Orogen tectonic evolution includes alternating periods of extension and compression (Griffin et al., 2000; Sheppard et al., 1999a; Kohanpour et al., 2017) and is considered to represent an accretionary orogen. As accretionary orogens and convergent margins are sites of complex alternating extensional and compressional regimes favourable to the development of gold and nickel mineral systems (Hronsky et al., 2012; Huston et al., 2016 and herein references), it is necessary to constrain the timing of tectonic events associated with nickel and gold mineralisation in the

evolution of the Halls Creek Orogen. In this study, Ar-Ar and Sm-Nd isotopic data are used to fill the gap in understanding the timing of mineralization and track the juvenile fertile zones in space and time for both nickel and gold mineral systems.

Age dating by the $^{40}\text{Ar}/^{39}\text{Ar}$ method on K-bearing minerals has been applied to some mineral deposits with a particular focus on gold deposits that have no direct links to the intrusive rocks for the application of U-Pb dating method (Bierlein et al., 2001; Foster et al., 1998). The $^{40}\text{Ar}/^{39}\text{Ar}$ method shows the time at which the K-bearing minerals cooled through a specific temperature interval (Kirkland and Wingate, 2012). The muscovite $^{40}\text{Ar}/^{39}\text{Ar}$ age indicates the time at which the region cooled from peak metamorphism through the muscovite closure temperature (c. $425 \pm 70^\circ\text{C}$ for a cooling rate of $10^\circ\text{C}/\text{Ma}$; 2σ ; recalculated by Scibiorski et al. (2015) using Monte Carlo simulations applied to the diffusion coefficients measured by Harrison et al. (2009) on crystals with similar dimension as investigated in this study. This is found to overlap with known orogenic gold mineralization that forms at greenschist facies (c. $300\text{--}450^\circ\text{C}$) to lower amphibolite facies (c. $<550^\circ\text{C}$) (Groves, 1993; Groves et al., 1998; Tomkins, 2015). Potassium metasomatism is also well documented to occur during Au mineralization (e.g. Phillips and Powell, 2009; Rice et al., 2016; Saunders and Tuach, 1991; Wilson et al., 2003), resulting in the crystallization of K feldspar, muscovite, sericite, and biotite. Thus the age of the muscovite may reflect the age of the hydrothermal process associated with gold mineralization.

The isotopic information also provides a constraint on the timing and nature of the source rock (i.e. juvenile or recycled), and hence on crustal growth (Champion and Cassidy, 2008; Champion and Sheraton, 1997; Griffin et al., 2004; Huston et al., 2014). One important isotopic system commonly used in studies of granites and related rocks is Sm-Nd, which provides a proxy for the source and model ages of the crustal blocks that

magmatic rocks occur within by looking at the secular and geographical changes of isotopic signatures (Champion, 2013). The Sm-Nd system was successfully used in the Yilgarn Craton, Western Australia to delineate crustal domains and their relationships with mineralisation (Cassidy et al., 2005; Huston et al., 2014; Mole et al., 2014). The 'juvenile' and 'evolved' concepts in reference to the isotopic source refer to more radiogenic or positive ϵNd , and less radiogenic or negative ϵNd (Huston et al., 2014). This assumption is consistent with the Nd records which show that a primitive and enriched mantle source differentiated into high Sm/Nd values reflecting a more radiogenic and depleted mantle. Low Sm/Nd values reflect a less radiogenic and thus evolved crust (Vervoort and Blichert-Toft, 1999). The two-stage Nd depleted mantle model age (T^2_{DM}) (Liew and McCulloch, 1985) is used to estimate the age of a sample (as a proxy for the crust in the region) has been separated from its mantle source (DePaolo, 1981). For granitoids derived from the melting of continental crust, the mantle model age can be explained as a mixing age of when the various components in the crustal source were separated from the mantle (Curtis and Thiel, 2019). Thus, the whole-rock Nd values can be used to identify the spatial gradients in age and composition of the deep sources of the granitoids (e.g. Albrecht and Goldstein, 2000; Hildreth and Moorbath, 1988; McDowell et al., 1999).

The newly acquired data in combination with our current understanding developed from geology, geodynamics, and geophysics is used to determine the mineral system components and corresponding mappable proxies in application with GIS-based prospectivity models. The results of this study show that there is a link between nickel and gold mineral systems within the Halls Creek Orogen through marginal basin development and subsequent basin closure. Although a general conceptual framework of mineral system analysis and prospectivity modelling presented by Occhipinti et al. (2016) is followed, significant advances in scientific understanding are included: (i) a newly defined geodynamic evolution of the

region (Kohanpour et al., 2017; Kohanpour et al., 2019); (ii) application of whole-rock Nd analysis as a proxy for terrane fertility for gold and nickel mineralization; and (iii) the first $^{40}\text{Ar}/^{39}\text{Ar}$ analysis of hydrothermal alteration associated with gold mineralization. The principal elements of mineral systems considered here as lithospheric architecture, geodynamic throttle, fertility, depositional sites, and preservation (Occhipinti et al., 2016), are translated to mappable criteria and applied to a knowledge-driven GIS-based fuzzy logic prospectivity analysis. This work addresses three main questions. (i) What are the main geological processes or critical factors that were most influential on gold and nickel endowment in the Halls Creek Orogen? (ii) Where are the prospective zones for gold and nickel mineralization within the region? (iii) Does the addition of isotopic datasets such as Sm-Nd and $^{40}\text{Ar}/^{39}\text{Ar}$ improve our understanding of mineral systems components and prospectivity analyses?

2. Regional geology

The Halls Creek Orogen (HCO) is a well-exposed Paleoproterozoic orogenic belt, extending along the eastern side of the Kimberley Craton margin (Fig. 1). This orogen provides insights into the collision of the Kimberley Craton with the Diamantina Craton during the amalgamation of the Nuna Supercontinent. The Halls Creek Orogen comprises three tectonostratigraphic terranes: the Western, Central, and Eastern zones (Tyler et al., 1995). These terranes are separated by major fault systems. The northeast-trending Angelo–Halls Creek–Osmond fault system separated the Central and Eastern zones. The Western and Central zones are separated by the northeasterly trending Ramsay Range and Springvale faults, and the northern part of the Halls Creek Fault (Fig. 1). These three zones contain distinct Paleoproterozoic geological units and were juxtaposed by the 1870–1850 Ma Hooper Orogeny and 1835–1805 Ma Halls Creek Orogeny (Griffin et al., 2000; Griffin and Tyler, 1992; Tyler et al., 1995). The later

deformation events which affect all three terranes are the c. 1000–800 Ma Yampi Orogeny, c. 560 Ma King Leopold Orogeny, and c. 370–300 Ma Alice Spring Orogeny.

The main lithological units of the Halls Creek Orogen are shown in Fig. 1. The Eastern Zone mainly consists of metasedimentary and metavolcanic rocks of the 1880–1840 Ma Halls Creek Group, which contains the Saunders Creek, Brim Rockhole, Biscay, and Olympio formations (Griffin and Tyler, 1992; Phillips et al., 2016). The turbiditic metasedimentary rocks of Olympio Formation contain trachyandesitic and trachytic rocks of the 1857 ± 5 Ma Maude Headley (Page and Hancock, 1988) and 1848 ± 3 Ma Butcher Gully Members (Blake et al., 1998). It was supposed that the metasedimentary and mafic rocks of the Halls Creek Group were deposited on the margin of North Australian Craton (Griffin et al., 2000). The Halls Creek Group is intruded by sills of c.1855–1835 Ma Woodward Dolerite (Griffin and Tyler, 1992; Phillips et al., 2016; Tyler et al., 1998). Rocks in the Eastern Zone were metamorphosed and variably deformed to greenschist facies (Occhipinti et al., 2016). The oldest rocks in the Central Zone are the c.1865 Ma mafic volcanic and turbiditic sedimentary rocks of Tickalara Metamorphics which were metamorphosed from greenschist to granulite facies (Tyler et al., 1995), and intruded by the tonalite and trondhjemite of the Dougalls Suite at 1850 Ma. A sequence of folded and metamorphosed turbidites, carbonate, mafic and felsic volcanoclastic rocks of the 1845–1840 Ma Koongie Park Formation is exposed in the southern part of the Central Zone (Tyler et al., 2012). The 1856–1830 Ma layered mafic-ultramafic intrusions observed in the Central Zone (Page and Hoatson, 2000). This zone was also extensively intruded by the felsic to mafic rocks of the 1835–1805 Ma Sally Downs Supersuite during the Halls Creek Orogeny. The main components of Western Zone are the c.1870 Ma turbiditic sedimentary rocks of the Marboo Formation, c.1855 Ma Whitewater Volcanics, and 1865–1850 Ma granitic and gabbroic rocks of the Paperbark Supersuite.

2.1. Gold and nickel mineralisation

The Halls Creek Orogen hosts a variety of mineral deposits documented by Sanders (1999) and Hassan (2000). The major known mineralisation styles are orogenic Au, Ni–Cu–PGE, VMS, porphyry-style Cu, REE deposits, and diamond-bearing intrusions. Metasedimentary and felsic volcanic rocks of the Halls Creek Group in the Eastern Zone contain gold deposits (Fig. 1) (Sanders, 1999). Gold mineralisation styles in the Eastern Zone consist of quartz-carbonate sulphide veins hosted in brittle-ductile shears (e.g. the Mount Bradley deposit), stockwork quartz veins hosted in trachyandesitic to syenitic rocks of the Butchers Gully Member (e.g. the Palm Spring deposit), and alluvial occurrences (Sanders, 1999). The Central Zone contains a few gold deposits in the late faults hosted by felsic volcanoclastic rocks of Koongie Park Formation, Loadstone Monzogranite and ultramafic rocks of the Lamboo intrusion in the Nicholsons Find area (Sanders, 1999).

Warrren (1997) suggested that gold mineralisation in the Eastern Zone was derived from the mafic volcanic rocks of the Biscay Formation, lower Olympio Formation or alkaline volcanic rocks of the Butchers Gully and Maude Headley members and then remobilized into late faults. Tyler et al. (1998) suggested that gold mineralisation is related to low-grade metamorphism and a deformation event associated with the c. 1000-800 Ma Yampi Orogeny. Kohanpour et al. (2018) established that the controlling structures are mainly attributed to the deformation events that occurred during the 1835–1805 Ma Halls Creek Orogeny plate convergence or subsequent strike-slip movement of c.1000–800 Ma Yampi Orogeny.

Significant Ni–Cu–PGE mineralisation is mainly restricted to layered mafic-ultramafic intrusions in the Central Zone of the Halls Creek Orogen (Occhipinti et al., 2016; Sanders, 1999) (Fig. 1). The 1856 ± 2 Ma Panton and 1844 ± 3 Sally Malay intrusions are understood to be the most

prospective intrusion for Ni–Cu–PGE mineralisation in areas dominated by amphibolite facies rocks of Tickalara Metamorphics in the Central Zone (Occhipinti et al., 2016). The mineralised mafic-ultramafic intrusions are spatially controlled by the intersection of deep crustal structures parallel with and orthogonal to the orogeny (Lindsay et al., 2016b), suggesting these structures acted as magma conduits (Occhipinti et al., 2016). The mineralised Panton and Sally Malay intrusions are folded by deformation events associated with 1835–1805 Ma Halls Creek Orogeny; therefore, intrusions of mafic-ultramafic rocks and nickel mineralisation took place prior to the accretion of Eastern Zone to the Central Zone (Sanders, 1999; Kohanpour et al., 2018).

2.2. Tectonic evolution of the Halls Creek Orogen

The tectonic evolution of the Halls Creek Orogen has been extensively investigated by chemical and isotope analysis of granites (Griffin et al., 2000; Sheppard et al., 1999a; Tyler et al., 2012). Griffin et al. (2000) and Sheppard et al. (1999a) considered the c.1865 Ma Tickalara Metamorphics as a key unit in the Central Zone to understand the tectonic evolution of the Halls Creek Orogen. The formation of the protholiths to the Tickalara Metamorphics have been described as either forming in (1) an oceanic island arc setting above an easterly dipping subduction outboard of Kimberley Craton; or (2) an ensialic marginal basin located at the margin of Kimberley Craton (Griffin et al., 2000; Sheppard et al., 1999a). The mentioned ambiguity in tectonic evolution of the Halls Creek Orogen has been evaluated by geodynamic numerical modelling (Kohanpour et al., 2017).

The results of numerical modelling suggest the Halls Creek Orogen formed by west-dipping subduction at the margin of the Kimberley Craton (Kohanpour et al., 2017). Using time-constrained Hf isotope ratios of zircon grains from the Halls Creek Orogen (Kohanpour et al., 2019) confirmed development of an extensional regime in the early stages of subduction, leading to the formation of a back-arc basin, which is postulated to be the tectonic setting for deposition of the precursor sedimentary and igneous rocks of the Tickalara Metamorphics. Subsequent decompression melting may have caused the intrusion of mafic-ultramafic rocks into the Halls Creek Orogen. Subduction was terminated by the collision of continental plates including the combined Western and Central zones at the margin of the Kimberley Craton with the North Australian Craton. In this model, collision resulted in compression and closure of the marginal basin. The final phase of the collision was marked by the intrusion and suturing of the North Australian and Kimberley cratons by mantle-derived magmatism (Model I in Kohanpour et al., 2017).

The Halls Creek Orogen tectonic evolution includes alternating periods of extension and compression (Fig. 2) (Kohanpour et al., 2017). The main geodynamic processes operating in the Halls Creek Orogen include crustal thinning in the early stage of subduction, whereas slab detachment and crustal thickening are the most important processes during the final stage of convergent margin settings or collisions. Therefore, the evolution of the orogen is divided into three stages: The first stage (Fig. 2a) is oceanic crust subduction which is accompanied by formation of a volcanic arc and back-arc basin. This stage involves a period of local extension and crustal thinning, accompanied by upwelling of decompression melt in the early stage of the convergence between two plates. This stage is followed by an intermediate stage (Fig. 2b) of orogeny during which the overriding plate undergoes compression due to the collision of two plates. In this phase, a switch from extension to compression occurs, accompanying with basin inversion and closure. The periods of anomalous compression and/or switch in tectonic regimes are the time when the geodynamics of the

region may impose strong threshold barriers to fluid flow, resulting in a highly-organised fluid flux in the system (McCuaig and Hronsky, 2014) (Fig. 2b). The final stage (Fig. 2c) of the convergent system is marked by slab detachment, relaxation of the crust, and mantle-derived syn- to post-collisional magmatism. In this study, the tectonic evolution of the Halls Creek Orogen was based on the numerical models of Kohanpour et al. (2017) after the conceptual models of Sheppard et al. (1999a) and Griffin et al. (2000). Other possible scenarios which considered the Kimberly Craton to be a part of a larger North Australian Craton are not considered here, although they need to define processes led to the injection of mantle-derived melts in the evolution of the Halls Creek Orogen based on the recent isotopic data (Kohanpour et al., 2019).

3. Methods

3.1. Ar-Ar analysis

In this study, we used the $^{40}\text{Ar}/^{39}\text{Ar}$ dating method on muscovite from hydrothermally altered samples in gold deposits to understand the time and the corresponding metallogenic events of orogenic gold mineralization in the context of the understood tectono-thermal development of the Halls Creek Orogen. Two samples from the trachyandesite rocks at the Mount Bradley Mine and quartz-sericite alteration zone within the Nicholsons Find Mine were analysed (Fig. 3). Crossed polar photomicrographs of typical muscovite crystals from the alteration zone associated with gold deposits are presented in Fig. 3 (a-d). The Mount Bradley deposit is hosted by trachyandesitic rocks of the Butchers Gully Member dated at 1848 ± 3 Ma (Blake et al., 1998). The ore-hosting rock comprises K-feldspar, plagioclase and minor quartz. The fine-grained recrystallised muscovite flakes replace K-feldspar and plagioclase, representing textural features associated with hydrothermal muscovite (Miller et al., 1981; Gomes and

Neiva, 2000) (Fig.3a-b). A strongly altered sample from the marginal alteration zone close to the quartz veins of Nicholsons Find Mine shows no preservation of igneous texture. The recrystallised quartz grains and muscovite flakes are the dominant minerals of the sample (Fig.3c-d).

Muscovite crystals ranging from 212 to 125 μm size fractions, were washed, dried and then hand-picked under a binocular microscope. Only transparent grains with less surface weathering were chosen for analysis. The selected grains were loaded into discs and irradiated for 80 hours at 1000 kw in a CLICIT (Cadmium Lined Inner Core Irradiation Tube) facility at the Oregon State University TRIGA reactor. The discs include a fully inter-calibrated FCs (Fish Canyon sanidine) standard with an age of 28.294 Ma (Renne et al., 2011). The main J-value (irradiation parameter) computed from standard grains within the small pits was $0.02167360 \pm 0.00001951$ for the Nicholsons Find Mine sample and $0.02167360 \pm 0.00001731$ for Mount Bradley sample. The correction factors for interfering isotopes were $(^{39}\text{Ar}/^{37}\text{Ar})_{\text{Ca}} = 7 \times 10^{-4} (\pm 1.2\%)$, $(^{36}\text{Ar}/^{37}\text{Ar})_{\text{Ca}} = 2.6 \times 10^{-4} (\pm 0.4\%)$ and $(^{40}\text{Ar}/^{39}\text{Ar})_{\text{K}} = 7.3 \times 10^{-4} (\pm 12.4\%)$ (Renne, 2013). The criteria for the determination of plateaus are as follow: the plateau must include at least 70% of ^{39}Ar and should be distributed over a minimum of three consecutive steps agreeing at 95% confidence level and satisfying a probability of fit (P) at least 0.05. Plateau ages from step-heated single-grain aliquots are reported with two-sigma uncertainties. All ages are calculated the decay constants proposed by Renne et al. (2011).

3.2. Sm-Nd analysis

In this study, we use whole-rock Nd isotopic data to decipher the geographical changes in isotopic signature across the Halls Creek Orogen. These data and resultant maps provide implications for juvenile and/or reworked sources of granites, as well as implications for the relations of isotopic

signatures with gold and nickel mineralization. A database of Sm-Nd isotopic data for 109 samples of the Halls Creek Orogen rocks was compiled from this study, published data (Griffin et al., 2000; Phillips et al., 2016; Sheppard et al., 2001; Sun and Hoatson, 2000), and unpublished data of Geological Survey of Western Australia online database (data source in Appendix 1). Data were compiled for a range of lithologies including felsic and mafic igneous rocks and sedimentary rocks which have reliable location details and a reasonable estimated or known magmatic age. The approach used here is different from the Champion (2013), as they used felsic and intermediate rock to investigate Australia's lithospheric architecture on a large scale, whereas we are going to track the juvenile (i.e. mantle-derived) rocks and their relations to gold and nickel mineral system in the Halls Creek Orogen. The locations of samples overlain with the geological map are shown in Appendix 2.

Nine samples of felsic and mafic intrusions across the Central Zone of the Halls Creek Orogen are analysed for this study. Sm-Nd isotopic values were determined on crushed whole-rock samples by isotope dilution. All analyses were carried out at the Géosciences Rennes Laboratory at the University of Rennes 1. Samples were spiked with a ^{150}Nd - ^{149}Sm mixed solution and dissolved in HF-HNO₃. REE elements were separated using BioRad AG 50W × 8 H + 200–400 mesh cationic resin. Sm and Nd were separated and collected by passing the solution through a further set of ion exchange columns loaded with Ln spec Eichrom resin. Sm and Nd were loaded with HNO₃ reagent on to double Re filaments and analysed in a Finnigan MAT262 multi-collector mass spectrometer in static mode. In each analytical session, the unknowns were analysed together with the Ames nNd-1Nd standard, which during the course of this study yielded an average of 0.511956 (standard deviation = 4.95×10^{-6}). All analyses of the unknowns are adjusted to a nominal $^{143}\text{Nd}/^{144}\text{Nd}$ value of 0.511850 for the La Jolla standard. Mass fractionation was monitored and corrected

using the value $^{146}\text{Nd}/^{144}\text{Nd} = 0.7219$. Procedural blanks analysed during the period of these analyses were ~ 100 pg and are considered to be negligible compared to the total quantity of Nd in the samples.

The calculated epsilon Nd (ϵNd), and two-stage model age (T^2_{DM}) values were used to generate isotopic maps across the Halls Creek Orogen by applying two approaches. The first involved gridding ϵNd and T^2_{DM} map generated in ArcMap by undertaking inverse distance weighted (IDW) interpolation with intervals based on natural breaks, i.e. intervals were calculated by the software. In addition, we used the geological maps to manually assign the calculated value or average of values of ϵNd and T^2_{DM} related to the mapped lithological units in the region and producing an interpreted map in Arc Map. Nd model age (T^2_{DM}) and ϵNd maps, besides T^2_{DM} /time and ϵNd /time plots, help us to decipher the secular and spatial changes of isotopic signatures of the crustal elements and place constraints on their possible source across the Halls Creek Orogen.

3.3. GIS prospectivity modelling

Mineral prospectivity modelling is a commonly used technique in integrating diverse datasets in regional exploration targeting (Bonham-Carter, 1994; Carranza, 2008). Mineral prospectivity models can be considered as mathematical functions that determine where multiple important geological features in a mineral system coincide (Occhipinti et al., 2016). Prospectivity models are generally classified into knowledge-driven and data-driven based on whether model parameters rely on geological criteria in the formation of mineral deposits or statistical relationships between the location of known mineral deposits and coincident geological features (Porwal et al., 2003). The optimal method of prospectivity analysis can be selected depending on the number of known deposits in a given region, but also the quality of the data and the confidence one may have in how

accurately these locations represent levels of mineralisation required by the explorer (Occhipinti et al., 2016). Knowledge-driven mineral prospectivity modelling coupled with mineral system analysis is more useful in areas with no or very few mineral deposits (Joly et al., 2014), or regions seemingly possessing a large number of data points, but which have been shown to be mis-representative of mineralisation and thus inappropriate for data-driven modelling methods (for example, Lindsay et al 2016a). Subsequently, knowledge-driven methods have been widely used in mineral prospectivity modelling in greenfield regions where mineral deposit data typically meet one or both the rejection criteria (An, 1991; Bonham-Carter, 1994; Carranza and Hale, 2000; D'Ercole et al., 2000; Joly et al., 2014; Joly et al., 2012; Knox-Robinson, 2000; Lindsay et al., 2016a; Occhipinti et al., 2016).

In this study, due to: (1) the limited number of known economic deposits in the Halls Creek Orogen; (2) the lack of confidence measures and field-validated assessment of the deposit location point data and; (3) the overarching aim of the study (translating the geological concepts into mineral systems components and prospectivity modelling), the knowledge-driven fuzzy logic approach has been used for creating mineral prospectivity maps of magmatic nickel sulfide and gold mineralisation. This approach needs an understanding of different mineral system components and their relative roles in the formation of ore deposits to define fuzzy membership values. Geodynamic evolution, geophysical and geological interpretation, and isotopic data obtained from the study area are integrated to understand mineral system components and define suitable mappable proxies (predictor maps) for all key elements important in the formation and preservation of nickel and gold deposits.

The fuzzy membership values for predictor maps are estimated from the map weights, class weights and confidence factors (Joly et al., 2014; Occhipinti et al., 2016). Map weights, class weights and confidence factors were assigned to the different predictor maps based on an understanding of different mineral systems and geological evolution of the Halls Creek Orogen. The subjectively derived fuzzy membership is a useful way of incorporating geological knowledge in the GIS-based automated methods (Lindsay et al., 2016a). Map weights are defined based on the importance of the predictor maps in mineral system analysis. Class weights indicate the spatial variations from prospective geological features, and in most cases, values are assumed to decrease linearly with distance from the object of interest to the edge of a buffer zone, a cut-off distance beyond which the influence of a feature is negligible. The buffer zone represents the maximum distance permitted to be prospective. Confidence factors were assigned to each predictor map based on its perceived ability to (1) define the appropriate component of a mineral system accurately, and (2) image the desired component in a raster/map form.

The fuzzy operators include OR, and PRODUCT used to produce mineral system components and final prospectivity maps. The fuzzy OR is a function that retains the highest value from a combination of predictor layers, and is useful when combining different layers within a component. The fuzzy PRODUCT is a penalty-function that returns the product of several fuzzy values which are less than one. Thus, fuzzy PRODUCT provides a way to combine values without simply returning the value of a dominant layer, while strongly penalizing input areas with low-fuzzy values. These aspects of fuzzy PRODUCT led to the choice of using it to combine values from different components of mineral systems (i.e. source, pathway, depositional traps, etc.) to model mineral prospectivity (Lindsay et al., 2016a).

The modelling followed the steps described by Lindsay et al. (2015) and Occhipinti et al. (2016) includes: (1) identifying mappable proxies for key components of a mineral system; (2) creating predictor maps based on the identified proxies; (3) classifying the predictor maps and assign map weight, class weight, and confidence factor to the predictor maps; (4) generating the prospectivity models through the overlay of weighted predictor maps in fuzzy inference network to produce mineral system components maps and final prospectivity maps. The classification approaches, map weights and confidence factors are presented in Table 1. It also depicts how the predictor maps combined to create maps for the mineral system components before proceeding to the final nickel and gold prospectivity maps. All of the models were constructed in ESRI ArcToolbox, by Model Builder and can be easily modified with different weights and operators.

4. Results

4.1. Timing of gold mineralization

A summary of the $^{40}\text{Ar}/^{39}\text{Ar}$ results appears in Table 2 and Appendix 3. Single-grain muscovite from an altered sample in Nicholsons Find Mine yielded a plateau age of 1826 ± 5 Ma (mean square weighted deviation, MSWD = 1.59, P = 0.08). Single-grain muscovite from a trachyandesite in Mount Bradley deposit yielded a plateau age of 1838 ± 5 Ma (MSWD = 1.56, P = 0.12). Plateau ages were calculated from our samples with > 98% and 74% ^{39}Ar released; and the mean ages are reported with 2σ uncertainty (Fig. 3 e-f). Here we consider that the plateau ages of the muscovite crystals represent the age of hydrothermal processes typically associated with gold mineralization. The isotopic results illustrate that the gold deposit formation occurred at 1838 Ma in Mount Bradley Mine in the Eastern Zone and 1826 Ma in Nicholsons Find Mine in the Central

Zone. Therefore, suggesting that gold mineralisation occurred during the early stage of 1835–1805 Ma Halls Creek Orogeny. This period corresponds to a tectonic switch from an extensional to a compressional regime which was related to basin closure (Kohanpour et al., 2017). Interpretation of the isotopic data suggests a westward migration of collision and accretion corresponding to a diachroneity in the timing of gold mineralisation between c.1838 Ma in the east to c.1826 Ma in the west. Similar interpretations have been formed from conceptual tectonic models (Griffin et al., 2000; Sheppard et al., 1999a), geodynamic numerical modelling (Kohanpour et al., 2017) and Lu/Hf data (Kohanpour et al., 2019).

4.2. Temporal and spatial patterns in Nd isotopes

The Nd isotopic signature of magmatic rocks records varying proportions of crustal melting versus juvenile mantle magma input in the Halls Creek Orogen (Figs. 4 and 5, Table 3 and Appendix 1). The full data of whole-rock Nd analysis from the samples across the Halls Creek Orogen is provided in Appendix 1, and the samples analysed for this study are presented in Table 3. Figs. 4a–b show gridded images of T^2_{DM} and ϵNd map, and Figs. 4c–d present the resulted maps from assigning the T^2_{DM} and ϵNd to the lithological units based on understanding their geological relationships (Fig. 4e) (Griffin and Tyler, 1992; Tyler et al., 1995; Tyler et al., 2012). The Nd signature is a function of either two end-member mixing scenarios, resulting from either the input of juvenile mantle material or reworking of an unradiogenic crustal source. Therefore, the gridded interpolation between different lithological units are not representative of isotopic signatures of major lithological units across the whole orogen, especially for the regions suffering from the lack of samples (Fig. 4a, sites A and B), and therefore, be disregarded. However, in the regions with sufficient whole-rock Nd data, the interpolation can map large-scale crustal architecture (Fig. 4a, sites C and D). The second approach which

assigns the ϵNd values to each lithological unit can provide more a more accurate assessment of the possible geographical distribution of isotopic signatures across the region.

The pre-1900 Ma magmatic rocks of the Eastern Zone include Sophie Downs Granites and Ding Dong Downs Volcanics have ϵNd ranging from -4.64 to 0.15 and T_{DM}^2 ranging from 2.8 to 2.4 Ga, recording the melting of the pre-existing Neoproterozoic basement. The ϵNd of metavolcanic rocks of the Brim Rockhole and Biscay formations range from -0.78 to 4.77 and younger T_{DM}^2 between 2.4 and 2 Ga suggesting more mantle inputs in their isotopic signature. The metasediments of the 1870–1840 Ma Olympio Formation and including trachytic rocks of the c. 1857 Ma Maude Headley Member have negative ϵNd ranging from -1.60 to -4.23 and T_{DM}^2 ranges from 2.7 to 2.5 Ga, recording the reworking and melting of the Neoproterozoic basement. The positive ϵNd value and T_{DM}^2 ranging from 2.3 to 2.1 (Ga) of the c.1835 Ma Woodward Dolerite suggesting a juvenile mantle-derived magma input.

The magmatic rocks that were deposited in the formed in the c.1865–1835 Ma Central Zone are dominantly crustally contaminated mantle-derived magmas resulting from lithospheric extension and upwelling of decompression melts (Fig. 2a) (Kohanpour et al., 2017). ϵNd values of the c.1865 Ma mafic metavolcanics of Tickalara Metamorphics vary from -0.6 to 5.69, and depleted mantle model ages for this unit are Paleoproterozoic, range from 2.4 to 1.9 Ga. The c. 1586–1830 Ma mafic-ultramafic units in the Central zone have ϵNd ranging from -1.13 to 4.17 (more samples with positive ϵNd values), and T_{DM}^2 ranging from 2.4 to 2 Ga, suggesting that the mantle source is likely similar in age and composition to the mafic components of Tickalara Metamorphics. The collisional magmatic rocks of the 1835–1805 Ma Sally Downs Supersuite contain more evolved

values of ϵNd (-3.21 to 1.46), and T_{DM}^2 ages between 2.6 and 2.3 Ga, suggesting that they are derived from a combination of a late Neoproterozoic crustal source region and juvenile mantle magma input.

The granitic and gabbroic intrusions of the 1865–1850 Ma Paperbark Supersuite in the Western Zone have evolved ϵNd values ranging from -3.09 to -1.14 with depleted mantle model ages ranging from 2.6–2.5 Ga, providing evidence of melting of a pre-existing Neoproterozoic crustal source. Similarly, the c.1855 Ma Whitewater Volcanics have negative ϵNd values (-3.9 and -4) and 2.7 Ga model ages. Interestingly, the mafic-ultramafic units of the Western Zone contain a different isotopic signature and model ages from the mafic-ultramafic units in the Central Zone. They have ϵNd values from -1.85 to 0.03, and T_{DM}^2 ages ranging from 2.5 to 2.37 Ga reflecting a crustal source.

The spatial pattern of Nd model ages (T_{DM}^2) across the region (Figs. 4c and 5a) highlights possible differences in the underlying crust from which the sampled lithological units were sourced. A significant change in Nd depleted mantle ages occurs in the Central Zone between the Halls Creek-Angelo and Springvale-Ramsay Range fault systems. There is a predominance of younger model ages from 2.4 to 1.9 Ga in the Central Zone, due to igneous rocks of Tickalara Metamorphics and mafic-ultramafic intrusions in this region, and also records a juvenile input. East of the Halls Creek Fault, the T_{DM}^2 ages range from 2.76 to 2.40 Ga, suggesting that the Neoproterozoic crust occurs in the subsurface beneath this region. However, Paleoproterozoic model ages are also observed for some igneous rocks in the Eastern Zone, suggesting juvenile inputs during the Paleoproterozoic. Similarly, in the Western Zone, the T_{DM}^2 ages range from 2.69 to 2.40 Ga, consistent with the presence of Neoproterozoic basement in this region. In summary, the Nd depleted mantle model ages across the Halls Creek Orogen suggest that major terrane boundaries separate Neoproterozoic basement

from more juvenile Paleoproterozoic rocks of the Central Zone (Fig. 4c). The 2.6–2.3 Ga T^2_{DM} model ages of the Sally Downs Supersuite, which formed during a collisional event, show the presence of Neoproterozoic basement during the Halls Creek Orogeny when suturing of the North Australian and Kimberley cratons occurred.

There is a generally well-correlated distribution of model ages with the known geology of the Halls Creek Orogen. The majority of Archean model ages (T^2_{DM}) are sampled from the Eastern and Western zones, and emplacement of younger model ages (T^2_{DM}) rocks in the Central Zone. The spatial pattern of ϵNd values (Figs. 4d and 5b) through the Halls Creek Orogen highlights the most juvenile signature (positive values) in the Central Zone. These juvenile units are created by upwelling of decompression mantle melt during the back-arc basin development at the margin of Kimberley Craton (Kohanpour et al., 2017). In addition, mafic and felsic igneous rocks of the Sally Down Supersuite represent evolved signature suggesting may be derived from a combination of the melting of a crustal source region (i.e. Neoproterozoic basement), as well as juvenile mantle magma inputs. The igneous rocks of Biscay and Brim Rockhole formations, and Woodward Dolerite in the Eastern Zone also show juvenile values.

4.3. Prospectivity models

4.3.1. Predictor maps

Source-Geodynamic throttle

In this study, the source component of the mineral system tied to the lithological units formed in metallogenically desirable tectonic settings during the much broader evolution of the Halls Creek Orogen. The reason for considering lithotype as a proxy for the source is that the origin of metal and fluid is connected to the processes of rocks formation. The lithological units are taken from the updated interpreted basement geological map (Occhipinti et al., 2016). A buffer zone of 1 km is considered around the lithological units. The map weights assigned to the different lithological units depend on their ability in providing metals and fluids in a particular tectonic setting.

Mafic-ultramafic units formed due to decompression mantle melting during marginal basin development (Fig. 2b) are assumed to have the greatest potential to host magmatic nickel sulfides. For example, the 1856 ± 2 Ma Panton and 1844 ± 3 Sally Malay intrusions which developed before the 1835-1805 Ma Halls Creek Orogeny. Relevant mafic-ultramafic rocks were extracted from the geological map as the source in nickel mineral system includes Sally Malay, Panton Suite, Toby gabbro, Springvale, Corridor gabbro, and Lamboo ultramafic. The highest weight of 1 was assigned to the known mineralized mafic-ultramafic units i.e. Sally Malay and Panton Suite in the Central Zone. The map weights of 0.8 and 0.7 were assigned to the other mafic-ultramafic units in the Western Zone and southern part of the Central Zone, respectively (Fig. 6a).

For the orogenic gold system, the metals and fluids are generally connected to the tectonic settings and are not considered to have any direct generic relationship to specific lithological units (Groves and Santosh, 2015). For this reason, we considered the lithological units within the perceived tectonic settings of orogenic gold deposits as the proxies for the source component. We used the lithological units related to three major possible tectono-magmatic environments for orogenic gold deposits and include sedimentary and volcanic rocks in the back-arc setting (Griffin et al., 2000; Occhipinti et al., 2016; Sheppard et al., 1999b), i.e. the Tickalara metamorphics and Koongie Park Formation, magmatic rocks of

collisional settings include felsic and mafic igneous rocks of Sally Downs Supersuite (Sheppard et al., 2001), and meta-volcanic and turbiditic sedimentary rocks of active margin origins (Tyler et al., 2012) which include the Olympio and Biscay formations (Fig. 6b). The map weights of lithological units are presented in Table 1. The ‘source’ predictor maps were combined using the fuzzy OR operator. A map weight of 0.9 was given to the ‘source’ component for the final fuzzy overlay.

Lithospheric architecture

The crustal-scale architecture is considered an essential component of gold and nickel mineral systems due to the critical role of faults in the regional-scale fluid migration (Cox et al., 2001; Groves et al., 1998; McCuaig and Hronsky, 2014). The regional structure interpretation by Kohanpour et al. (2017) was used as the source layer of structural features. Terrane boundaries are considered as the major mantle-tapping structures and are thus assigned the highest map weight of 1. A 10 km buffer zone is created around the terrane boundaries to simulate the potential for distal processes around the object. All major deep structures not considered to be terrane boundaries were considered during the analysis (Kohanpour et al., 2018) and assigned a 5 km buffer zone, as fluid pathways in the area. Major structures were divided into north-northeasterly or orogen-parallel and northwesterly cross-orogen segments. The NNE trending structures were assigned the map weight 0.8 since it considered they developed during the extensional phase of the accretionary orogen (Kohanpour et al., 2018). Whereas the NW striking structures were assigned a map weight of 0.7. The classes for all the predictor maps correspond to 1 km intervals, thus the membership values decrease from the maximum value away from the structure at 1 km intervals. The reclassified distance to faults and terrane boundaries combined using the fuzzy OR operator to generate the ‘lithospheric architecture’ map (Fig. 7). A map weight of 0.7 was given to the ‘lithospheric architecture’ component.

Depositional sites

Lower order structures and geological complexities in the middle to upper crust can act as physical traps for fluid (Breeding and Ague, 2002; Cox et al., 2001). Faults are prime locations for increased permeability that can trigger the fluid flow (Cox et al., 2001; Micklethwaite et al., 2010). Anticlinal folds axes also act as traps for mineralizing fluids (Groves et al., 2016; Kohanpour et al., 2018). Therefore, we created predictor maps ‘distance to faults’ with 1 km buffer zone and ‘distance to folds’ with 5 km buffer zone (Fig. 8a–b) to constrain the prospectivity to a specific distance beyond which the influence is considered negligible. Fault bends can also increase fluid flow in the system and act as depositional zones (Ford et al., 2009; Occhipinti et al., 2016). The ‘faults bends’ map generated by kernel density of point features representing changes in the orientation of faults (Fig. 8c). The density map of ‘geological complexities’ calculated as the kernel density of intersections of all line features including lithological boundaries, non-major faults and fold axes considered as a proxy for zones of localized damage and increased permeability (Fig. 8d). Lithological boundaries with high rheological and chemical reactivity contrasts are considered as preferential traps (Brown, 2002) and corresponding predictor maps were created. The assigned relative rheology and chemical reactivity value of the lithological units of the Halls Creek Orogen by Occhipinti et al. (2016) was used for creating predictor maps. Lithological contacts were attributed the difference values of respective rheological and geochemical reactivity values of two adjacent units, then the kernel density of contacts with contrast values larger than zero was computed for predictor maps of ‘competency contrast’ and ‘chemical reactivity contrast’ respectively (Fig. 8e, f). The kernel density tool in ArcGIS uses a window function to represent the magnitude-per-unit area of point feature density as a property value in the resulting output raster cell.

The ‘depositional sites’ map for magmatic nickel sulfide was generated using a fuzzy OR operator to combine the predictor maps geological complexity, competency contrast, and chemical reactivity contrast. Each predictor map was assigned a weight of 0.8 (Fig. 9a). The ‘depositional sites’ map for orogenic gold was generated by combining the predictor maps distance to folds, distance to fold axes, fault bends, geological complexities, competency contrast, and chemical reactivity contrast with map weights of 0.8, 0.9, 0.9, 0.7, 0.8, and 0.8, respectively (Fig. 9b). A map weight of 0.5 was assigned to the ‘depositional sites’ component.

Fertility

The relationship between nickel and gold deposits and more juvenile isotopic signature in the Halls Creek Orogen is apparent in Fig. 10a, suggesting that the isotopes may record the favourable tectonic settings for this mineralization in extensional zones which characterised by fluxes of juvenile magmas. While considering the role of mantle-derived magmatism in gold and nickel mineralization (Barnes et al., 2016; Bleeker, 2015; Blewett et al., 2010; Griffin et al., 2013; Hronsky et al., 2012; Wyman et al., 2016), and the close spatial correlation between the gold and nickel mineralized region in the Halls Creek Orogen with regional positive ϵNd signatures, we choose rocks with more juvenile signature (i.e. more radiogenic) as the more fertile rocks in mineral systems prospectivity analysis.

The ϵNd map was used as a proxy for fertility component in prospectivity modelling. Firstly, the ϵNd map is classified based on the values of ϵNd assigned to different lithological units, with the highest class values assigned to more juvenile rock types. We assigned the class value of 3 to ϵNd values greater than 1.5, 2 to values between 0 and 1.5, 1 to values between -2.16 and 0, and 0 to values less than -2.16 (Fig. 10b). Map weights of 0.5 were given to the ‘fertility’ component due to lack of samples in some regions. It is noted that mineral system approach is based on a wide

range of geological information, and isotopic map such as the ϵNd image presented in this section is just one layer that will be integrated with 'source' layer to present the lithological units that provide ore components for mineralisation.

Preservation

The preservation component is critical for some types of mineral systems, especially for those formed in the upper crust. In this study, metamorphic maps created by Occhipinti et al. (2016) were used as a proxy for preservation (Fig. 11a). The metamorphic map also presents the sharp boundaries between low/medium and high metamorphic along the major faults. The configuration of metamorphic grade of outcropping units suggests structurally controlled exhumation of fault blocks (Lindsay et al., 2016b). Magmatic nickel sulfide deposits tend to form at a wide range of crustal depths (Barnes et al., 2016), therefore the preservation component is not used for the prospectivity model. Orogenic gold deposits are formed in crustal depths from 3 to 20 km (Groves, 1993), so preservation is an important consideration for prospectivity analysis. Based on the likelihood of gold deposits in the different metamorphic grades, we assigned the class values of 3 to 'greenschist facies', 2 to 'prehnite to greenschist facies' rocks, 1 to 'greenschist to amphibolite facies' and 'non-metamorphosed' rocks, and 0 to granulite and amphibolite rocks (Fig. 11b). A map weight of 0.5 was given to the 'preservation' component.

4.3.2. Fuzzy logic models

Fuzzy logic modelling is completed by combining predictor maps using an appropriate fuzzy inference network resulting in the generation of prospectivity maps. The fuzzy predictor maps of the source, lithospheric architecture, depositional sites, fertility, and preservation were first

combined using the fuzzy OR operator to create a single predictor map for each critical component of gold and nickel mineral system. Finally, the fuzzy map for each component of gold and nickel mineral systems, respectively, were combined using the fuzzy PRODUCT operator to create the output prospectivity maps (Figs. 12 and 13). Details of the fuzzy inference network used are presented in Table 1.

Nickel prospectivity model- Nickel prospectivity analysis was completed taking into account rock type, fertility, connectivity to deep crustal faults, depositional sites (i.e. areas with geological complexities, high rheological and chemical reactivity contrasts). Mafic-ultramafic rocks that intruded during the extensional event prior to the Halls Creek Orogeny such as the Pantom Suite, Sally Malay Suite, Toby Gabbro, Corridor Gabbro, Springvale Suite, and Lamboo ultramafic are included in this analysis. All prospective areas are within mapped mafic and ultramafic rocks. Therefore, proximity to mafic-ultramafic rocks as a source component of the mineral system has a major influence on the prospectivity calculations (Fig. 12). The resulting prospectivity map illustrates that deposits and occurrences of nickel sulfide have been captured in the prospectivity model (Fig. 12), with the addition of other areas not currently known to contain any nickel mineralization in the south of the Central Zone.

Gold prospectivity models- Unlike the Ni prospectivity analyses, the gold prospectivity model was completed with the addition of the preservation proxy. The source proxies included rock types that are considered to be formed during the marginal basin development and subsequent basin closure and collision, connectivity to deep structures and terrane boundaries, and depositional sites i.e. areas with structural complexities, anticlinal hinge zones, and dilational jogs. The Eastern zone appears to be the most prospective area for gold mineralization, but the highly prospective zone appears focused along the Halls Creek-Angelo faults system (Fig. 13a). This fault system is a terrane boundary between the Eastern and Central zones, reactivated through time and thus it could have been the focus of fluid through the region at periods coincident with basin formation and

closure. In the Eastern Zone, parts of the Biscay Formation in the regions of high structural complexities or areas around the shear zones between the major strike-slip faults are considered the most prospective regions (Fig. 13b). There is a cluster of gold deposits that are not highlighted in the prospectivity model in site A of figure 13b. This may be due to the lack of nearby mapped deep crustal-scale structures, although this area has a good potential for deposition, preservation, and source. Some high prospective regions are also located in the intersection of major deep structures, that could act as conduits for mineralizing fluids into the crust (Fig. 13c), or close to anticlinal structures for focusing the mineralizing fluids (Fig. 13c). In addition to the Eastern Zone, some areas in the Central Zone were found to be prospective for gold mineralisation. For example, in areas of greenschist facies Tickalara Metamorphics that contain favourable structural traps and are close to the deep structures (Fig. 13c). In the southern part of the Halls Creek Orogen, prospective regions coincide with juvenile isotopic signatures (Fig. 13a) derived from intrusions of Lamboo Ultramafics and Woodward Dolerite. Interestingly, many regions considered prospective for Au mineralization area in the Central Zone are in areas with no known Au mineralisation and highlight further mineral exploration opportunities.

5. Discussion

The prospective areas of nickel and gold mineralization modelled in the Halls Creek Orogen lie in the Central Zone and Eastern Zone and are mainly controlled by tectonic processes, which have been recognized by integrating the geodynamic model, geophysical interpretation and isotopic data from the region. Three metallogenically important tectono-magmatic environments for magmatic nickel and orogenic gold mineralisation are recognized in the Halls Creek Orogen. The first is the superimposed rift (back-arc basin) on the active convergent margin as a response to slab

rollback and upwelling of mantle decompression melt. Rifting and juvenile magma input to the margin of Kimberley Craton is confirmed by a positive ϵNd signature in the Central Zone, whereas the evolved values resulting from reworking of Archean basement are observed in the Eastern and Western zones. A range of gold deposits and magmatic Ni sulfide deposits may form in this environment (Barnes et al., 2016; Hronsky et al., 2012). These rifts are dominated by sedimentary and magmatic rocks characterized by relatively high-temperature/low-pressure metamorphic assemblages in continental margins, as observed in the Halls Creek Orogen (Occhipinti et al., 2016). Whereas the mafic magmatic rocks locally provide the Ni and other important elements, sedimentary rocks deposited in this setting are likely to have provided a source of sulfur (Barnes et al., 2016).

The second metallogenic environment is associated with inversion of a continental rift during a switch from extension to compression. Orogenic gold deposits can be one of the main mineralization-styles developed in this environment (Bleeker, 2015; Blewett et al., 2010; Hagemann et al., 2016; Hronsky et al., 2012; Huston et al., 2016; Wyman et al., 2016). Basin inversion is sometimes associated with the transition from mafic mantle-derived to crustal-derived magmatism that can be synchronous with gold mineralisation (Cassidy et al., 2002; Champion and Cassidy, 2007, 2008; Czarnota et al., 2010). This transition is clear in the ϵNd values when the juvenile signatures of Tickalara Metamorphics and mafic-ultramafic units changed to more evolved values of Sally Downs Supersite. In addition, Ar-Ar dating of gold mineralization suggests that orogenic gold deposits in the Halls Creek Orogen formed subsequent to basin formation, in the early stage of collision when closure of the marginal basin occurred.

The third major tectono-magmatic environment is characterized by upwelling of the hydrated mantle that generates bimodal volcanism during continental collision and likely triggers formation of magmatic Ni sulfide deposits (Begg et al., 2010). Ni-PGE mineralized mafic-ultramafic intrusions including the c. 1856 Ma Panton and c. 1845 Ma Sally Malay Suites (Hoatson, 2000) were deformed during the 1835-1805 Ma Halls Creek Orogeny (Kohanpour et al., 2018) suggesting that nickel mineralisation occurred prior to this event. Extensional environments are accepted as being a common setting for nickel sulfide mineralization deposition (Begg et al., 2010; Naldrett, 2004) providing the right conditions for moderate to high degrees of partial melting beneath continents in regions of the thinned lithosphere (Dulfer et al., 2016). However, mildly compressional or transpressional conditions for Ni-PGE deposition have also been suggested by Begg et al. (2010). The lack of crustal contamination and juvenile signatures (positive ϵNd values) of mineralised mafic-ultramafic units in the Central Zone suggest that upwelling of mantle-derived melts and crustal thinning in an extensional environment could lead to the development of nickel mineralisation in the Hall Creek Orogen. Although, the possibility of Ni-PGE mineralization in the early stage of collision when basin inversion and regional compression were dominant, cannot be disregarded as it is reported in some nickel mineralization hosted by small intrusions (Begg et al., 2010 and herein references).

Although the magmatic nickel mineral system can be directly linked to the mafic-ultramafic units in the extensional setting, the areas of highest Au prospectivity modelled in the Halls Creek Orogen cannot be directly linked to the lithological units and their corresponding tectonic settings. In case of considering the possibility of the formation and preservation of orogenic gold deposits in amphibolite facies and granulite terranes (Groves et al., 1998; Lisitsin and Pitcairn, 2016; McCuaig et al., 1993; Vielreicher et al., 2016) the preservation layer can be discarded from the

prospectivity modelling. In this case, the resulting prospectivity map suggests that the metamorphosed rocks of the Tickalara Metamorphics in the Central Zone which formed in the marginal (back-arc) basin appear to be the most prospective areas for orogenic gold deposits (Fig. 14a).

Furthermore, in order to understand the importance of fertility for orogenic gold targeting, we completed the prospectivity analysis without including a fertility layer. The resulting map highlights a large prospective area across the region, mainly based on the structural controls (Fig. 14b), and illustrates that addition of isotopic/geochemical data as a proxy for fertility to the prospectivity model can make a significant difference in constraining the gold prospective regions. This may be due to isotopic signatures highlighting large-scale geodynamic processes and source of magmatism involved in mineralisation. It is demonstrated that applying geochemical and/or isotopic fertility indicators can restrict the extent of the prospective areas, which is desirable for exploration targeting.

Another considered factor in the prospectivity of orogenic gold deposit is the source, which is still hotly controversial because the potential sources could be distal (hundreds of km) to the depositional sites (Tomkins, 2015; Groves and Santosh, 2015; Groves et al., 2016;). To test the influence of the source layer, it was removed from prospectivity modelling. The resulting map (Fig. 14c) does not show significant changes in comparison with the main prospectivity model presented in Fig. 13. This may be due to the possibility of a wide range of lithological units as a source component for gold mineralization. It should be noted that some more small prospective regions in Western and Eastern zones appeared due to proximity to deep structures and fertility values. Although we applied a high map weight for the source layer, its contribution in the final prospectivity model is not noticeable, suggesting the significance of other mineral system components, especially fertility and structural controls in the targeting of the orogenic gold deposits.

Results for the nickel and gold prospectivity models show that the most influential critical element for the prospectivity is fertility, herein mapped using isotopic data, but previously mapped using lithological data alone (Occhipinti et al., 2016). It is demonstrated that the ϵNd map is a significant evidence layer that can reflect the tectono-magmatic environments of nickel and gold mineral systems. This is the case even though this critical element layer was not highly weighted in the final fuzzy overlay (Table. 1). The source which is correlated to the lithological units has a critical role for nickel mineralization, whereas it is not so influential for orogenic gold prospectivity model. Major crustal-scale shear zones and faults acting as fluid pathways and structural traps. They may play a more important role in the orogenic gold mineral system than the source component. The process of generating a prospectivity analysis drove simultaneous consideration of the results gained from geodynamic modelling, geophysical interpretation, and isotope analysis, thus revealed links between nickel and gold mineral systems. Evidence of deep connectivity to mantle-sourced melts is interpreted from the geological features associated with both nickel and gold mineralization. These features are deep and crustal-scale structures representing fluid pathways, and juvenile rocks representing mantle-sourced melts. The age of gold mineralisation (1838–1826 Ma, during the early stages of the 1835–1805 Ma Halls Creek Orogeny) and intrusion of prospective nickel sulfide-bearing mafic-ultramafic rocks before c.1835 Ma illustrate that nickel and gold mineralisation are correlated with the marginal basin development and subsequent basin closure. A transition from basin development to closure resulted in nickel to gold producing system in the Halls Creek Orogen. Basin development and upwelling of mantle-derived melts, development and reactivation of deep crustal faults and exhumation of the crust (Lindsay et al., 2016b) are the critical processes common to the formation, preservation, and spatial distribution of both nickel and gold deposits across the Halls Creek Orogen.

The results also exhibit the effectiveness of the knowledge-driven GIS-based prospectivity modelling in reducing the search space for explorers (Lindsay et al., 2016). Tables 4 and 5 show the reduction in search space achieved by this study. If the top three percentiles (i.e. highest 50%) of the prospectivity values are considered to be the most attractive sites for explorers, then this analysis reduced the search space to 3.2% and 2.2% of the total of the study area for gold and nickel mineral systems, respectively. Conversely, if the lowest 50% of prospectivity values are considered unprospective, the analysis shows that approximately 95% of the study area can be ignored for gold and nickel exploration. In geographical terms, this reduces the area of the ground for further studies at camp scales to 742 km² for orogenic gold and 517 km² for magmatic nickel mineralisation from an initial study area of 23067 km². Applying isotopic mapping to prospectivity modelling reduces the search space efficiently from 1583 km² to 742 km², an improvement of almost 50%, for targeting orogenic gold deposits. However, the source component is not as effective and does not reduce the search space considerably (Table 5). The metamorphic layer, as a proxy of preservation, is moderately effective and reduces the search space from 953 km² to 742 km², but more importantly, relocates highly prospective regions from the Central Zone to the Eastern Zone (Fig. 14a and Table 5). These results highlight how important isotopic mapping is for the techniques applied in this study. This can be extended to prospectivity modelling in general, and potential benefit isotopic data can provide in reducing the search space in greenfield regions.

6. Conclusions

This study has sought to develop a deeper understanding of mineral system components in the Halls Creek Orogen by applying the geodynamic numerical models, geological-geophysical interpretations, and isotopic analysis. Theoretical concepts and criteria for each of the five mineral systems components including geodynamic throttle, lithospheric architecture, fertility, depositional sites, and preservation were analyzed and

evidence maps generated to best represent favourable geological processes that led to nickel and gold mineralisation. For the first time, the age of gold mineralization is determined in the Halls Creek Orogen. In addition, the whole-rock Nd analysis across the region used to produce the fertility map by applying an interpretive method rather than gridding. The resultant Nd-fertility map allowed us to employ isotopic inputs in the prospectivity analysis.

The geodynamic models and isotopic data clarify the link between major tectono-metallogenic events with nickel and gold mineralization. A better understanding of geodynamic settings and tectonic evolution has led us to a greater understanding of large-scale controls on mineral systems, which resulted in greater predictive ability. The isotopic analysis ($^{40}\text{Ar}/^{39}\text{Ar}$ and whole-rock Nd) and deformational overprints used to determine the specific tectonic events and lithological units responsible for nickel and gold mineralisation. The lithological units developed in the metallogenically favourable geodynamic epochs provide the source component for prospectivity analysis. Furthermore, whole-rock Nd analysis provides the spatial distribution of fertilized regions, especially for the orogenic gold mineral systems that source component is not robust. The major crustal-scale faults are shown to control the regional distribution of nickel and gold deposits. Of these, terrane boundaries seem to be the most influential structures which are implied to be sites of fluid migration across the region.

The effectiveness of available datasets as proxies for the mappable criteria is an issue in any GIS-based knowledge-driven prospectivity modelling. This has been addressed as far as possible by assigning weightings consistent with the importance and reliability of the datasets. For this reason, we used a low weight for isotopic datasets due to the irregular distribution of data across the region. It is recognized the additional geochemical and isotopic data could significantly change the assessment of prospectivity models by providing fertility indicators across the region.

Prospectivity modelling shows the most favorable areas for magmatic nickel sulfides are in the Central Zone associated with mantle-derived mafic-ultramafic rocks that lie close to deep crustal-faults. Prospectivity modelling of orogenic gold deposits shows a strong relationship with structural traps within the mantle-derived rocks (i.e. Biscay Formation, Woodward Dolerite, and Tickalara Metamorphics) in the Eastern and Central zones with particular favorability along the Halls Creek-Angelo faults system. The results highlighted that the syn-orogenic extensional regime accompanied by upwelling of mantle-derived melts, and the following compressional regime and basin closure are the critical processes in the formation of the nickel and gold deposits.

Acknowledgment

This work is part of MRIWA Project, M465 “Deep crustal-scale structure, geological evolution, and multi-commodity analysis in the Halls Creek Orogen, Kimberley region, Western Australia”. ML is supported by and ARC DECRA (DE190100431), the DARE ARC ITTC (IC190100031) and the ‘MinEx’ CRC. We would like to thank the Geological Survey of Western Australia, Panoramic Resource Ltd and MRIWA for their financial, field, and data support. We thank Andy Wilde and an anonymous reviewer for helpful comments.

Figure Captions

Fig.1. Simplified map of major lithological units, and structures of the Lamboo Province; sites of known gold deposits and nickel occurrences from MINEDEX plotted on the map.

Fig. 2. Three main geodynamic processes in the Halls Creek orogen (Kohanpour et al., 2017). (a) Oceanic crust subduction, slab pull, and extensional regime led to basin development and upwelling of decompression melt; (b) Switch from extension to compression result in basin

closure; (c) Slab detachment, hydrated of mantle melt and collisional magmatism. (KC and NAC refer to Kimberley and North Australian cratons, respectively).

Fig. 3. Photomicrographs of typical muscovite/sericite crystals from the hydrothermally altered samples associated with gold deposits: (a-b) Trachyandesitic rocks of the Butcher Gully Member, very small flakes of recrystallised muscovite replacing K-feldspar and the groundmass; (c-d) A sample marginal to quartz veins in Nicholsons Find Mine representing pervasive silicification and sericitization with no preservation of primary igneous texture of igneous host rocks. $^{40}\text{Ar}/^{39}\text{Ar}$ muscovite age plateaus from the gold deposits in the Halls Creek Orogen, (e) Mount Bradley deposit; (f) Nicholsons Find Mine. ms = muscovite, qtz = quartz, kfs = K-feldspar.

Fig. 4. T^2_{DM} and ϵNd maps of the Halls Creek Orogen, (a-b) generated by inverse distance weighted (IDW) interpolation in ArcMap; (c-d) created by assigning the calculated values to the lithological units. Location of the samples, isotopic data, and the crystallization age of the related lithological units superimposed over the maps (Data are in Appendix 1). Grid colour in areas without samples are purely based on interpolation and cannot show the isotopic signature of the underlying crust. (a and c) The T^2_{DM} maps present the lithological units in the Central Zone with the crystallization ages of (1865-1835 Ma) show younger model ages, while the samples with Archean model age are mainly located in the Eastern and Western zones. (b and d) The figures present the juvenile magma inputs (positive ϵNd) in the centre of the Orogen, and in some igneous rocks of the Eastern Zone. The lithological units with crystallisation ages of c.1865-1835 Ma are more juvenile and have younger model age.

Fig. 5. (a) Magmatic age versus model age (T^2_{DM}) for samples in the Halls Creek Orogen, suggests reworking of Neoproterozoic basement in the Eastern and Western zones and younger crustal growth mainly in the Central Zone. (b) Magmatic age versus epsilon Nd (ϵNd), shows the Western and Eastern zones have more evolved isotopic signature, whereas juvenile mantle input mainly occurred in the Central Zone. Fields show the evolution of Neoproterozoic basement and Halls Creek rocks through time.

Fig. 6. Representative maps of 'source' for magmatic nickel sulfide (a) and orogenic gold (b) mineralization styles resulting from the fuzzy algebraic OR of distance to selected lithological units based on their tectonic settings.

Fig. 7. Representative map of 'lithospheric architecture', resulting from a fuzzy algebraic OR of terrane boundaries and major deep structures with buffer distances of 10 km for terrane boundaries and 5km for major structures.

Fig. 8. Evidence layers used as proxies for 'depositional site': (a) distance to non-major faults; (b) distance to fold axis; (c) kernel density of fault bends; (d) geological complexities calculated as kernel density of faults and lithological units; (e) kernel density of rheological contrast; (f) kernel density of chemical reactivity contrast.

Fig. 9. Representative maps of ‘depositional sites’ for magmatic nickel sulfide (a), and orogenic gold deposits (b), calculated from fuzzy overlays of evidence layers presented in Fig. 8.

Fig. 10. (a) Location of gold and nickel deposits in the Halls Creek Orogen, superimposed over the ϵNd values of the lithological units. A strong correlation of mineralization to a juvenile signature is observed. (b) Classified map of the spatial pattern of ϵNd used as a proxy for ‘fertility’ component.

Fig. 11. (a) Map of the regional metamorphic grade of lithological units of the Halls Creek Orogen (Occhipinti et al., 2016); (b) Representative map of ‘preservation’ used for the final fuzzy overlay of orogenic gold prospectivity models.

Fig. 12. Prospectivity map derived for magmatic nickel sulfide mineralization overlain with nickel mines, deposits and occurrences, presenting a close relationship of highly prospective areas with mafic-ultramafic units as ‘source’ component.

Fig. 13. Prospectivity maps for orogenic gold mineralization in the Halls Creek Orogen overlain with Au deposits and mines, (a) Regional scale prospectivity map illustrating that the highest prospectivity is within the Eastern Zone; (b & c) Enlarged maps representing the relations of high prospective areas with interpreted structures from Kohanpour et al. (2018) and major lithological units.

Fig. 14. (a) Gold prospectivity models that consider gold deposits forming in amphibolite-granulite metamorphic conditions; (b) Prospectivity maps produced without the ‘fertility’ component. This is similar to previous results presented by Occhipinti et al. (2016); (c) Prospectivity map produced without the ‘source’ component. This result is comparable with the model presented in Fig. 13a, suggesting the source layer cannot make significant differences in gold prospectivity.

Table Captions

Table 1. Fuzzy inference network for nickel and gold prospectivity modelling; Halls Creek Orogen.

Table 2. $^{40}\text{Ar}/^{39}\text{Ar}$ muscovite results from the gold deposits, Halls Creek Orogen.

Table 3. New Sm-Nd data for selected Paleoproterozoic units across the Halls Creek Orogen.

Table 4. Search area reduction statistics.

Table 5. Search area reduction statistics for orogenic gold deposit prospectivity models

Appendices

Appendix 1. Compilation of Sm-Nd data across the Halls Creek Orogen (includes: this study, Sheppard et al., 2001; Griffin et al., 2000; Sun and Hoatson, 2000, unpublished data from GSWA, Geoview website).

Appendix 2. Geographical distribution of Sm-Nd samples on the geological map of the Halls Creek Orogen; the numbers present sample “Id” in Appendix 1.

Appendix 3. Full data table of $^{40}\text{Ar}/^{39}\text{Ar}$ results.

References

Albrecht, A., and Goldstein, S. L., 2000. Effects of basement composition and age on silicic magmas across an accreted terrane-Precambrian crust boundary, Sierra Madre Occidental, Mexico: *Journal of South American Earth Sciences*, v. 13, no. 3, p. 255-273.

An, P., 1991. Application of fuzzy set theory to integrated mineral exploration: *Can. J. Explor. Geophys.*, v. 27, p. 1-11.

Barnes, S. J., Cruden, A. R., Arndt, N., and Saumur, B. M., 2016. The mineral system approach applied to magmatic Ni–Cu–PGE sulphide deposits: *Ore Geology Reviews*, v. 76, p. 21.

Begg, G. C., Hronsky, J. A. M., Arndt, N. T., Griffin, W. L., O’Reilly, S. Y., and Hayward, N., 2010. Lithospheric, Cratonic, and Geodynamic Setting of Ni-Cu-PGE Sulfide Deposits: *Economic Geology*, v. 105, no. 6, p. 1057-1070.

Bierlein, F., Arne, D., Foster, D., and Reynolds, P., 2001. A geochronological framework for orogenic gold mineralisation in central Victoria, Australia: *Mineralium Deposita*, v. 36, no. 8, p. 741-767.

Blake, D.H., Tyler, I.M., Griffin, T.J., Sheppard, S., Thorne, A.M., Warren, R.G., 1998. Geology of the Halls Creek 1:100 000 Sheet, Western Australia. Australian Geological Survey Organisation, Canberra.

- Bleeker, W., 2015. Synorogenic gold mineralization in granite-greenstone terranes: the deep connection between extension, major faults, synorogenic clastic basins, magmatism, thrust inversion, and long-term preservation: Geological Survey of Canada, Open File, v. 7852, p. 25-47.
- Blewett, R. S., Henson, P. A., Roy, I. G., Champion, D. C., and Cassidy, K. F., 2010. Scale-integrated architecture of a world-class gold mineral system: The Archaean eastern Yilgarn Craton, Western Australia: *Precambrian Research*, v. 183, no. 2, p. 230-250.
- Bonham-Carter, G. F., 1994. Geographic information systems for geoscientists : modelling with GIS, Kidlington [Oxfordshire], Pergamon, Computer methods in the geosciences; v. 13.
- Breeding, C. M., and Ague, J. J., 2002. Slab-derived fluids and quartz-vein formation in an accretionary prism, Otago Schist, New Zealand: *Geology*, v. 30, no. 6, p. 499-502.
- Brown, W. M., 2002. Artificial neural networks: a new method for mineralprospectivity mapping: PhD thesis, v. unpublished, p. 368.
- Carranza, E. J. M., 2008. Geochemical anomaly and mineral prospectivity mapping in GIS, Elsevier.
- Carranza, E. J. M., and Hale, M., 2000, Geologically Constrained Probabilistic Mapping of Gold Potential, Baguio District, Philippines: *Natural Resources Research*, v. 9, no. 3, p. 237-253.
- Cassidy, K. F., Champion, D. C., and Huston, D. L., 2005. Crustal evolution constraints on the metallogeny of the Yilgarn Craton, *in Proceedings Mineral Deposit Research: Meeting the Global Challenge 2005*, Springer, p. 901-904.
- Cassidy, K. F., Champion, D. C., McNaughton, N. J., Fletcher, I. R., Whitaker, A. J., Bastrakova, I. V., and Budd, A. R., 2002. Characterisation and metallogenic significance of Archaean granitoids of the Yilgarn Craton, Western Australia: Minerals and Energy Research Institute of Western Australia (MERIWA), Report, no. 222, p. 514.
- Champion, D. C., 2013. Neodymium depleted mantle model age map of Australia: explanatory notes and user guide, Geoscience Australia.
- Champion, D. C., and Cassidy, K. F., 2007. An overview of the Yilgarn Craton and its crustal evolution: *Geoscience Australia Record*, v. 14, p. 8-13.
- Champion, D. C., and Cassidy, K. F., 2008. Geodynamics: using geochemistry and isotopic signatures of granites to aid mineral systems studies: an example from the Yilgarn Craton: *Geoscience Australia, Record*, p. 7-16.

Champion, D. C., and Sheraton, J. W., 1997. Geochemistry and Nd isotope systematics of Archaean granites of the Eastern Goldfields, Yilgarn Craton, Australia: implications for crustal growth processes: *Precambrian Research*, v. 83, no. 1, p. 109-132.

Cox, S., Knackstedt, M., and Braun, J., 2001. Principles of Structural Control on Permeability and Fluid Flow in Hydrothermal Systems: *Reviews in Economic Geology*, v. 14, p. 1-24.

Curtis, S., and Thiel, S., 2019. Identifying lithospheric boundaries using magnetotellurics and Nd isotope geochemistry: An example from the Gawler Craton, Australia: *Precambrian Research*, v. 320, p. 403-423.

Czarnota, K., Champion, D. C., Goscombe, B., Blewett, R. S., Cassidy, K. F., Henson, P. A., and Groenewald, P. B., 2010. Geodynamics of the eastern Yilgarn Craton: *Precambrian Research*, v. 183, no. 2, p. 175-202.

D'Ercole, C., Groves, D. I., and Knox-Robinson, C. M., 2000. Using fuzzy logic in a Geographic Information System environment to enhance conceptually based prospectivity analysis of Mississippi Valley-type mineralisation: *Australian Journal of Earth Sciences*, v. 47, no. 5, p. 913-927.

DePaolo, D. J., 1981. Neodymium isotopes in the Colorado Front Range and crust–mantle evolution in the Proterozoic: *Nature*, v. 291, p. 193.

DePaolo, D. J., and Wasserburg, G. J., 1976. Nd isotopic variations and petrogenetic models: *Geophysical Research Letters*, v. 3, no. 5, p. 249-252.

Dulfer, H., Milligan, P. R., Coghlan, R., Czarnota, K., Highet, L. M., Champion, D. C., and Skirrow, R. G., 2016. Potential for Intrusion-hosted Ni-Cu-PGE Sulfide Deposits in Australia: A Continental-scale Analysis of Mineral System Prospectivity, *Geoscience Australia*.

Ford, A., Blenkinsop, T. G., and McLellan, J. G., 2009. Factors affecting fluid flow in strike–slip fault systems: coupled deformation and fluid flow modelling with application to the western Mount Isa Inlier, Australia: *Geofluids*, v. 9, no. 1, p. 2-23.

Foster, D. A., Gray, D. R., Kwak, T. A. P., and Bucher, M., 1998. Chronology and tectonic framework of turbidite-hosted gold deposits in the Western Lachlan Fold Belt, Victoria: 40 Ar – 39 Ar results: *Ore Geology Reviews*, v. 13, no. 1, p. 229-250.

Gomes, M. E. P., Neiva, A. M. R., 2000. Chemical zoning of muscovite from the Ervedosa granite, northern Portugal: *Mineralogical Magazine*, v.64, no.2, p. 347-358.

Griffin, T. J., Page, R. W., Sheppard, S., and Tyler, I. M., 2000. Tectonic implications of Palaeoproterozoic post-collisional, high-K felsic igneous rocks from the Kimberley region of northwestern Australia: *Precambrian Research*, v. 101, no. 1, p. 1-23.

Griffin, T. J., and Tyler, I. M., 1992. Geology of the southern Halls Creek Orogen: a summary of field work in 1992, Geological Survey of Western Australia, Record 1992/17, p. 28.

Griffin, W. L., Begg, G. C., and O'Reilly, S. Y., 2013. Continental-root control on the genesis of magmatic ore deposits: *Nature Geoscience*, v. 6, p. 905.

Griffin, W. L., Belousova, E. A., Shee, S. R., Pearson, N. J., and O'Reilly, S. Y., 2004. Archean crustal evolution in the northern Yilgarn Craton: U–Pb and Hf-isotope evidence from detrital zircons: *Precambrian Research*, v. 131, no. 3, p. 231-282.

Groves, D. I., 1993. The crustal continuum model for late-Archaean lode-gold deposits of the Yilgarn Block, Western Australia: *Mineralium Deposita*, v. 28, no. 6, p. 366-374.

Groves, D. I., Goldfarb, R. J., Gebre-Mariam, M., Hagemann, S. G., and Robert, F., 1998. Orogenic gold deposits: A proposed classification in the context of their crustal distribution and relationship to other gold deposit types: *Ore Geology Reviews*, v. 13, no. 1–5, p. 7-27.

Groves, D. I., Goldfarb, R. J., and Santosh, M., 2016. The conjunction of factors that lead to formation of giant gold provinces and deposits in non-arc settings: *Geoscience Frontiers*, v. 7, no. 3, p. 303-314.

Groves, D. I., and Santosh, M., 2015. Province-scale commonalities of some world-class gold deposits: Implications for mineral exploration: *Geoscience Frontiers*, v. 6, p. 389-399.

Hagemann, S. G., Lisitsin, V. A., and Huston, D. L., 2016. Mineral system analysis: Quo vadis: *Ore Geology Reviews*, v. 76, p. 504-522.

Harrison, T. M., Célérier, J., Aikman, A. B., Hermann, J., and Heizler, M. T., 2009. Diffusion of ⁴⁰Ar in muscovite: *Geochimica et Cosmochimica Acta*, v. 73, no. 4, p. 1039-1051.

Hassan, L., 2000, Mineral occurrences and exploration potential of the east Kimberley: Geological Survey of Western Australia no. 74, p. 83.

Hildreth, W., and Moorbath, S., 1988. Crustal contributions to arc magmatism in the Andes of Central Chile: *Contributions to Mineralogy and Petrology*, v. 98, no. 4, p. 455-489.

Hoatson, D. M. a. B., D. H., 2000. Geology and economic potential of the Paleoproterozoic layered mafic-ultramafic intrusions in the East Kimberley, Western Australia., *in* Organization, A. G. S., ed., p. 499.

Hronsky, J., Groves, D., Loucks, R., Begg, G., Hronsky, J., Groves, D., Loucks, R., and Begg, G., 2012. A unified model for gold mineralisation in accretionary orogens and implications for regional-scale exploration targeting methods: *Miner Deposita*, v. 47, no. 4, p. 339-358.

Huston, D. L., Champion, D. C., and Cassidy, K. F., 2014. Tectonic Controls on the Endowment of Neoproterozoic Cratons in Volcanic-Hosted Massive Sulfide Deposits: Evidence from Lead and Neodymium Isotopes: *Economic Geology*, v. 109, no. 1, p. 11-26.

Huston, D. L., Mernagh, T. P., Hagemann, S. G., Doublier, M. P., Fiorentini, M., Champion, D. C., Lynton Jaques, A., Czarnota, K., Cayley, R., Skirrow, R., and Bastrakov, E., 2016. Tectono-metallogenic systems — The place of mineral systems within tectonic evolution, with an emphasis on Australian examples: *Ore Geology Reviews*, v. 76, p. 168-210.

Joly, A., Aitken, A. R. A., Dentith, M., Porwal, A., Smithies, R. H., and Tyler, I. M., 2014. Mineral Systems Analysis of the West Musgrave Province: Regional Structure and Prospectivity Modelling, Geological Survey of Western Australia.

Joly, A., Porwal, A., and McCuaig, T. C., 2012. Exploration targeting for orogenic gold deposits in the Granites-Tanami Orogen: Mineral system analysis, targeting model and prospectivity analysis: *Ore Geology Reviews*, v. 48, no. 0, p. 349-383.

Kirkland, C. L., and Wingate, M. T. D., 2012. Reading deep time: radiogenic isotope geochronology: Geological Survey of Western Australia, v. Record 2012/15, p. 10.

Knox-Robinson, C. M., 2000. Vectorial fuzzy logic: A novel technique for enhanced mineral prospectivity mapping, with reference to the orogenic gold mineralisation potential of the Kalgoorlie Terrane, Western Australia: *Australian Journal of Earth Sciences*, v. 47, no. 5, p. 929-941.

Knox-Robinson, C. M., and Wyborn, L. A. I., 1997. Towards a holistic exploration strategy: Using Geographic Information Systems as a tool to enhance exploration: *Australian Journal of Earth Sciences*, v. 44, no. 4, p. 453-463.

Kohanpour, F., Gorczyk, W., Lindsay, M. D., and Occhipinti, S., 2017. Examining tectonic scenarios using geodynamic numerical modelling: Halls Creek Orogen, Australia: *Gondwana Research*, v. 46, p. 95-113.

Kohanpour, F., Kirkland, C. L., Gorczyk, W., Occhipinti, S., Lindsay, M. D., Mole, D., and Le Vaillant, M., 2019. Hf isotopic fingerprinting of geodynamic settings: Integrating isotopes and numerical models: *Gondwana Research*, v. 73, p. 190-199.

Kohanpour, F., Lindsay, M. D., Occhipinti, S., and Gorczyk, W., 2018. Structural controls on proterozoic nickel and gold mineral systems identified from geodynamic modelling and geophysical interpretation, east Kimberley, Western Australia: *Ore Geology Reviews*, v. 95, p. 552-568.

Kreuzer, O. P., Markwitz, V., Porwal, A. K., and McCuaig, T. C., 2010. A continent-wide study of Australia's uranium potential: Part I: GIS-assisted manual prospectivity analysis: *Ore Geology Reviews*, v. 38, no. 4, p. 334-366.

Liew, T. C., and McCulloch, M. T., 1985. Genesis of granitoid batholiths of Peninsular Malaysia and implications for models of crustal evolution: Evidence from a Nd/Sr isotopic and U/Pb zircon study: *Geochimica et Cosmochimica Acta*, v. 49, no. 2, p. 587-600.

Lindsay, M., Aitken, A., Ford, A., Dentith, M., Hollis, J., and Tyler, I., 2016a. Reducing subjectivity in multi-commodity mineral prospectivity analyses: Modelling the west Kimberley, Australia: *Ore Geology Reviews*, v. 76, p. 395-413.

Lindsay, M., Aitken, A. R. A., Ford, A., Dentith, M., Hollis, J. A., Tyler, I. M., and Geological Survey of Western, A., 2015. Mineral prospectivity of the King Leopold Orogen and Lennard Shelf: potential field analysis in the West Kimberley / MD Lindsay, AR Aitken, A Ford, MC Dentith, JA Hollis, IM Tyler, East Perth, W.A, Geological Survey of Western Australia.

Lindsay, M. D., Occhipinti, S., Aitken, A. R. A., Metelka, V., Hollis, J., and Tyler, I., 2016b. Proterozoic accretionary tectonics in the east Kimberley region, Australia: *Precambrian Research*, v. 278, p. 265-282.

Lisitsin, V. A., and Pitcairn, I. K., 2016. Orogenic gold mineral systems of the Western Lachlan Orogen (Victoria) and the Hodgkinson Province (Queensland): Crustal metal sources and cryptic zones of regional fluid flow: *Ore Geology Reviews*, v. 76, no. C, p. 280-295.

McCuaig, T. C., Beresford, S., and Hronsky, J., 2010. Translating the mineral systems approach into an effective exploration targeting system: *Ore Geology Reviews*, v. 38, no. 3, p. 128-138.

McCuaig, T. C., and Hronsky, J. M. A., 2014. The mineral system concept: the key to exploration targeting: *Society of Economic Geologists, Special Publication*, v. 18, p. 153-175.

McCuaig, T. C., Kerrich, R., Groves, D. I., and Archer, N., 1993. The nature and dimensions of regional and local gold-related hydrothermal alteration in tholeiitic metabasalts in the Norseman goldfields: the missing link in a crustal continuum of gold deposits?: *Mineralium Deposita*, v. 28, no. 6, p. 420-435.

McDowell, F. W., Housh, T. B., and Wark, D. A., 1999. Nature of the crust beneath west-central Chihuahua, Mexico, based upon Sr, Nd, and Pb isotopic compositions at the Tomóchic volcanic center: *GSA Bulletin*, v. 111, no. 6, p. 823-830.

Micklethwaite, S., Sheldon, H. A., and Baker, T., 2010. Active fault and shear processes and their implications for mineral deposit formation and discovery: *Journal of Structural Geology*, v. 32, no. 2, p. 151-165.

Miller, C.F., Stoddard, E.F., Bradfish, L.J., and Dollase, W.A., 1981. Composition of plutonic muscovite; genetic implications. *The Canadian Mineralogist*, v.19, no.1, p.25-34.

Mole, D. R., Fiorentini, M. L., Thebaud, N., Cassidy, K. F., McCuaig, T. C., Kirkland, C. L., Romano, S. S., Doublier, M. P., Belousova, E. A., Barnes, S. J., and Miller, J., 2014. Archean komatiite volcanism controlled by the evolution of early continents: *Proceedings of the National Academy of Sciences*, v. 111, no. 28, p. 10083-10088.

Naldrett, A. J., 2004. *Magmatic sulfide deposits: Geology, geochemistry and exploration*, Springer Science & Business Media.

Occhipinti, S. A., Metelka, V., Lindsay, M. D., Hollis, J. A., Aitken, A. R. A., Tyler, I. M., Miller, J. M., and McCuaig, T. C., 2016. Multicommodity mineral systems analysis highlighting mineral prospectivity in the Halls Creek Orogen: *Ore Geology Reviews*, v. 72, Part 1, p. 86-113.

Page and Hancock, 1988. Geochronology of a rapid 1.85–1.86 Ga tectonic transition: Halls Creek orogen, Northern Australia: *Precambrian Research*, v. 40–41, p. 447-467.

Page, R. W., and Hoatson, D. M., 2000. Geochronology of the mafic-ultramafic intrusions. In: Hoatson, D. M., Blake, D. H. (Eds), *Geology and Economic Potential of the Paleoproterozoic Layered Mafic-Ultramafic Intrusions in the East Kimberley, Western Australia* Australian Geological Survey Organization Bulletin 246, pp. 163-172.

Phillips, C., Orth, K., Hollis, J., Kirkland, C., Bodorkos, S., Kemp, A., Wingate, M., Lu, Y., Iaccheri, L., and Page, R., 2016. Geology of the Eastern Zone of the Lamboo Province, Halls Creek Orogen, Western Australia.

Phillips, G. N., and Powell, R., 2009. Formation of gold deposits: Review and evaluation of the continuum model: *Earth-Science Reviews*, v. 94, no. 1–4, p. 1-21.

Porwal, A., and Carranza, E. J. M., 2015. Introduction to the Special Issue: GIS-based mineral potential modelling and geological data analyses for mineral exploration: *Ore Geology Reviews*, v. 71, p. 477-483.

Porwal, A., Carranza, E. J. M., and Hale, M., 2003. Artificial Neural Networks for Mineral-Potential Mapping: A Case Study from Aravalli Province, Western India: *Natural Resources Research*, v. 12, no. 3, p. 155-171.

Renne, P. R., 2013. Some footnotes to the optimization-based calibration of the $^{40}\text{Ar}/^{39}\text{Ar}$ system: Geological Society, London, Special Publications, v. 378, no. 1, p. 21-31.

Renne, P. R., Balco, G., Ludwig, K. R., Mundil, R., and Min, K., 2011. Response to the comment by W.H. Schwarz et al. on “Joint determination of ^{40}K decay constants and $^{40}\text{Ar}^*/^{40}\text{K}$ for the Fish Canyon sanidine standard, and improved accuracy for $^{40}\text{Ar}/^{39}\text{Ar}$ geochronology” by P.R. Renne et al. (2010): *Geochimica et Cosmochimica Acta*, v. 75, no. 17, p. 5097-5100.

Rice, C. M., Mark, D. F., Selby, D., Neilson, J. E., and Davidheiser-Kroll, B., 2016. Age and geologic setting of quartz vein-hosted gold mineralization at Curraghinalt, Northern Ireland; implications for genesis and classification: *Economic Geology and the Bulletin of the Society of Economic Geologists*, v. 111, no. 1, p. 127-150.

Sanders, T. S., 1999. Mineralization of the Halls Creek Orogen, East Kimberley region Western Australia, Geological Survey of Western Australia, Report 66, p. 44.

Saunders, C. M., and Tuach, J., 1991. Potassic and sodic alteration accompanying gold mineralization in the Rattling Brook Deposit, western White Bay, Newfoundland Appalachians: *Economic Geology and the Bulletin of the Society of Economic Geologists*, v. 86, no. 3, p. 555-569.

Scibiorski, E., Tohver, E., and Jourdan, F., 2015. Rapid cooling and exhumation in the western part of the Mesoproterozoic Albany-Fraser Orogen, Western Australia: *Precambrian Research*, v. 265, p. 232-248.

Sheppard, S., Griffin, T. J., and Page, I. M. T. R. W., 2001. High- and low-K granites and adakites at a Palaeoproterozoic plate boundary in northwestern Australia: *Journal of the Geological Society*, v. 158, p. 547-560.

Sheppard, S., Thorne, A. M., and Tyler, I. M., 1999a. Geology of the Bow 1:100 000 sheet, 1:100 000 Geological Series Explanatory Notes, Geological Survey of Western Australia, p. 36.

Sheppard, S., Tyler, I. M., Griffin, T. J., and Taylor, W. R., 1999b. Palaeoproterozoic subduction-related and passive margin basalts in the Halls Creek Orogen, northwest Australia: *Australian Journal of Earth Sciences*, v. 46, no. 5, p. 679-690.

Sun, S., and Hoatson, D. M., 2000. Trace-element geochemical and Nd isotopic study of the mafic -ultramafic intrusions: implications for their petrogenesis and tectonic environment-. In: Hoatson, D. M., Blake, D. H. (Eds), *Geology and Economic Potential of the Paleoproterozoic Layered Mafic-Ultramafic Intrusions in the East Kimberley, Western Australia* Australian Geological Survey Organization Bulletin 246, pp. 226-250.

Tomkins, A. G., 2015. On the source of orogenic gold: *Geology*, v. 41, no. 12, p. 1255-1256.

Tyler, I. M., Griffin, T. J., Page, R. W., and Shaw, R. D., 1995. Are there terranes within the Lamboo Complex of the Halls Creek Orogen?, Geological Survey of Western Australia. *Annual Review 1993-94*, vol. 1993/94, pp.37-46.

Tyler, I. M., Griffin, T. J., and Sheppard, S., 1998. Geology of the Dockrell 1:100 000 sheet, 1:100 000 Geological Series Explanatory Notes, Geological Survey of Western Australia, p. 24.

Tyler, I. M., Hocking, R. M., and Haines, P. W., 2012. Geological evolution of the Kimberley region of Western Australia, Geological Survey of Western Australia. Episode 35 (1). pp.298-306.

Vervoort, J. D., and Blichert-Toft, J., 1999. Evolution of the depleted mantle: Hf isotope evidence from juvenile rocks through time: *Geochimica et Cosmochimica Acta*, v. 63, no. 3, p. 533-556.

Vielreicher, N. M., Groves, D. I., and McNaughton, N. J., 2016. The giant Kalgoorlie Gold Field revisited: *Geoscience Frontiers*, v. 7, no. 3, p. 359-374.

Warren, R. G., 1997. Reconnaissance geological mapping in Dixon, SE McIntosh and northernmost Halls Creek 1: 100 000 sheet areas, East Kimberley, WA 1992-3, Australian Geological Survey Organisation.

Wilson, A. J., Cooke, D. R., and Harper, B. L., 2003. The Ridgeway gold-copper deposit: A high-grade alkalic porphyry deposit in the Lachlan fold belt, New South Wales, Australia: *Economic Geology*, v. 98, no. 8, p. 1637-1666.

Wyborn, L. A. I., Heinrich, C. A., and Jaques, A. L., 1994. Australian Proterozoic mineral systems: essential ingredients and mappable criteria. [abs.]. In: Hallenstein, P.C. (Ed.), *Australian Mining Looks North — the Challenges and Choices*: Australian Institute of Mining and Metallurgy Publication, v. 5, p. 7.

Wyman, D. A., Cassidy, K. F., and Hollings, P., 2016. Orogenic gold and the mineral systems approach: Resolving fact, fiction and fantasy: *Ore Geology Reviews*, v. 78, p. 322-335.

Table 1. Fuzzy inference network for nickel and gold prospectivity modelling; Halls Creek Orogen

| | <i>Mineral System Component</i> | <i>Predictor map</i> | <i>Buffer</i> | <i>Num. classes</i> | <i>Class division</i> | <i>Confidence factor</i> | <i>Map Weight</i> | <i>Fuzzy number</i> | <i>Fuzzy operator</i> | |
|-------------------------------------|----------------------------------|---------------------------------|---------------|---------------------|-----------------------|--------------------------|-------------------|---------------------|-----------------------|----|
| Orogenic Gold Mineral System | <i>Source</i> | Tickalara Metamorphics | 1000 | 3 | 1000 | 1 | 0.9 | 0.9 | OR | OR |
| | | Koongie Park Formation | 1000 | 3 | 1000 | 1 | 0.9 | 0.9 | | |
| | | Dougalls Suite | 1000 | 3 | 1000 | 0.8 | 0.9 | 0.72 | OR | |
| | | Sally Downs Supersuite (mafic) | 1000 | 3 | 1000 | 0.8 | 0.9 | 0.72 | | |
| | | Sally Downs Supersuite (felsic) | 1000 | 3 | 1000 | 0.72 | 0.9 | 0.65 | OR | |
| | | Biscay Formation | 1000 | 3 | 1000 | 0.63 | 0.9 | 0.57 | | |
| | | Olympio Formation | 1000 | 3 | 1000 | 0.7 | 0.9 | 0.63 | | |
| | | Woodward Dolerite | 1000 | 3 | 1000 | 0.7 | 0.9 | 0.63 | | |
| | <i>Lithospheric Architecture</i> | Distance to terrane boundaries | 10000 | 11 | 1000 | 1 | 0.7 | 0.7 | OR | |
| | | Distance to major NE structures | 5000 | 6 | 1000 | 0.7 | 0.7 | 0.49 | | |
| | | Distance to major NW structures | 5000 | 6 | 1000 | 0.8 | 0.7 | 0.56 | | |
| | <i>Depositional sites</i> | Distance to non-major faults | 1000 | 6 | 200 | 0.8 | 0.5 | 0.4 | OR | |
| | | Distance to fold hinges | 5000 | 11 | 500 | 0.9 | 0.5 | 0.45 | | |
| | | Geological complexities | NA | 11 | NA | 0.7 | 0.5 | 0.35 | | |
| | | Fault bends density | NA | 11 | NA | 0.9 | 0.5 | 0.45 | | |
| | | Rheological contrast | NA | 11 | NA | 0.8 | 0.5 | 0.4 | | |
| | | Chemical reactivity contrast | NA | 11 | NA | 0.8 | 0.5 | 0.4 | | |
| | <i>Fertility</i> | ENd map | NA | 4 | NA | 0.7 | 0.5 | 0.35 | | |
| | <i>Preservation</i> | Metamorphic map | NA | 4 | NA | 0.7 | 0.5 | 0.35 | | |

Table 1. Continued.

| | <i>Mineral System Component</i> | <i>Predictor map</i> | <i>Buffer</i> | <i>Num. classes</i> | <i>Class division</i> | <i>Confidence factor</i> | <i>Map Weight</i> | <i>Fuzzy number</i> | <i>Fuzzy operator</i> |
|--------------------------------|----------------------------------|---------------------------------|---------------|---------------------|-----------------------|--------------------------|-------------------|---------------------|-----------------------|
| Magmatic Nickel Sulfide | <i>Source</i> | Sally Malay Suite | 1000 | 3 | 1000 | 1 | 0.9 | 0.9 | <i>OR</i> |
| | | Panton Suite | 1000 | 3 | 1000 | 1 | 0.9 | 0.9 | |
| | | Springvale Suite | 1000 | 3 | 1000 | 0.8 | 0.9 | 0.72 | |
| | | Toby Gabbro | 1000 | 3 | 1000 | 0.8 | 0.9 | 0.72 | |
| | | Corridor Gabbro | 1000 | 3 | 1000 | 0.7 | 0.9 | 0.63 | |
| | | Lamboos Ultramafic | 1000 | 3 | 1000 | 0.7 | 0.9 | 0.63 | |
| | <i>Lithospheric Architecture</i> | Distance to terrane boundaries | 10000 | 11 | 1000 | 1 | 0.7 | 0.7 | <i>OR</i> |
| | | Distance to major NE structures | 5000 | 6 | 1000 | 0.7 | 0.7 | 0.49 | |
| | | Distance to major NW structures | 5000 | 6 | 1000 | 0.8 | 0.7 | 0.56 | |
| | <i>Depositional sites</i> | Geological complexities | NA | 11 | NA | 0.8 | 0.5 | 0.4 | <i>OR</i> |
| | | Rheological contrast | NA | 11 | NA | 0.8 | 0.5 | 0.4 | |
| | | Chemical reactivity contrast | NA | 11 | NA | 0.8 | 0.5 | 0.4 | |
| | <i>Fertility</i> | ENd map | NA | 4 | NA | 0.7 | 0.5 | 0.35 | |

Table 2. $^{40}\text{Ar}/^{39}\text{Ar}$ muscovite results from the gold deposits, Halls Creek Orogen.

| <i>Sample</i> | <i>Mineral</i> | <i>Size fraction (μm)</i> | <i>Plateau age ($\text{Ma} \pm 2\sigma$)</i> | ^{39}Ar (%) | <i>MSWD</i> | <i>P</i> | <i>n</i> |
|-----------------|----------------|---|---|----------------------|-------------|----------|----------|
| Mont Bradley | Muscovite | < 212 > 125 | 1838 \pm 5 | 74 | 1.56 | 0.12 | 10 |
| Nicholsons Find | Muscovite | < 212 > 125 | 1826 \pm 5 | 98 | 1.59 | 0.08 | 14 |

MSWD: mean squared weighted deviation; *P*: P-value; *n*: number of steps used in plateau.

Table 3. New Sm-Nd data for selected Paleoproterozoic units across the Halls Creek Orogen

| Sample ID | Lithological unit | UTM easting | UTM northing | Age (Ma) | Sm (ppm) | Nd (ppm) | $^{143}\text{Nd}/^{144}\text{Nd}$ | $^{147}\text{Sm}/^{144}\text{Nd}$ | $^{143}\text{Nd}/^{144}\text{Nd}_{(i)}$ | $\epsilon\text{Nd}_{(i)}$ | T_{CHUR} (Ga) | T_{DM} (Ga) | T_{DM}^2 (Ga) |
|------------|---|-------------|--------------|----------|----------|----------|-----------------------------------|-----------------------------------|---|---------------------------|------------------------|----------------------|------------------------|
| Kimb16-03 | Tickalara Metamorphics - Metagranite | 397363 | 8061557 | 1865 | 10.60 | 51.69 | 0.511737 | 0.1240 | 0.510216 | -0.16 | 1.88 | 2.41 | 2.39 |
| Kimb16-04 | Tickalara Metamorphics -Basalt | 393742 | 8054129 | 1865 | 2.91 | 9.69 | 0.512618 | 0.1814 | 0.510393 | 3.31 | — | 2.55 | 2.11 |
| Kimb16-08A | Mabel Downs Tonalite - Mafic inclusions | 391033 | 8062785 | 1832 | 4.20 | 24.91 | 0.511505 | 0.1020 | 0.510276 | 0.18 | 1.82 | 2.25 | 2.34 |
| Kimb16-08B | Mabel Downs Tonalite | 391033 | 8062785 | 1832 | 1.97 | 14.02 | 0.511283 | 0.0850 | 0.510258 | -0.18 | 1.84 | 2.22 | 2.36 |
| Kimb16-09 | Sally Downs Supersuite - Granitodiorite | 377914 | 8059399 | 1830 | 7.42 | 48.02 | 0.511348 | 0.0934 | 0.510230 | -0.91 | 1.90 | 2.29 | 2.42 |
| Kimb16-10 | Sally Downs Supersuite - Gabbro | 377930 | 8059355 | 1830 | 3.32 | 14.34 | 0.511951 | 0.1399 | 0.510276 | -0.06 | 1.84 | 2.49 | 2.35 |
| Kimb16-25 | Lamboou Ultramafic | 323947 | 7957031 | 1830 | 0.27 | 1.12 | 0.512080 | 0.1473 | 0.510306 | 0.71 | 1.72 | 2.48 | 2.29 |
| Kimb16-27 | Emul Gabbro | 319508 | 7959303 | 1830 | 0.69 | 2.20 | 0.512639 | 0.1902 | 0.510349 | 1.55 | — | 3.39 | 2.22 |
| Nic-04 | Koongie Park -Mafic volcanics | — | — | 1845 | 3.91 | 17.40 | 0.511900 | 0.1357 | 0.510254 | 0.06 | 1.84 | 2.46 | 2.36 |

T_{CHUR} (Ga) calculated assuming $^{143}\text{Nd}/^{144}\text{Nd}_{\text{CHUR}(0)} = 0.512638$ and $^{147}\text{Sm}/^{144}\text{Nd}_{\text{CHUR}(0)} = 0.1967$.

T_{DM} (Ga) calculated assuming $^{143}\text{Nd}/^{144}\text{Nd}_{\text{DM}(0)} = 0.513163$ and $^{147}\text{Sm}/^{144}\text{Nd}_{\text{DM}(0)} = 0.2136$.

T_{DM}^2 (Ga) calculated after the method of Liew and McCulloch (1985), assuming a $^{147}\text{Sm}/^{144}\text{Nd}$ ratio of average continental crust 0.12.

Age is the considered age for the lithological units based on the GSWA reports; Decay constant of $^{147}\text{Sm} = 6.54 \times 10^{-12}$.

Table 4. Search area reduction statistics

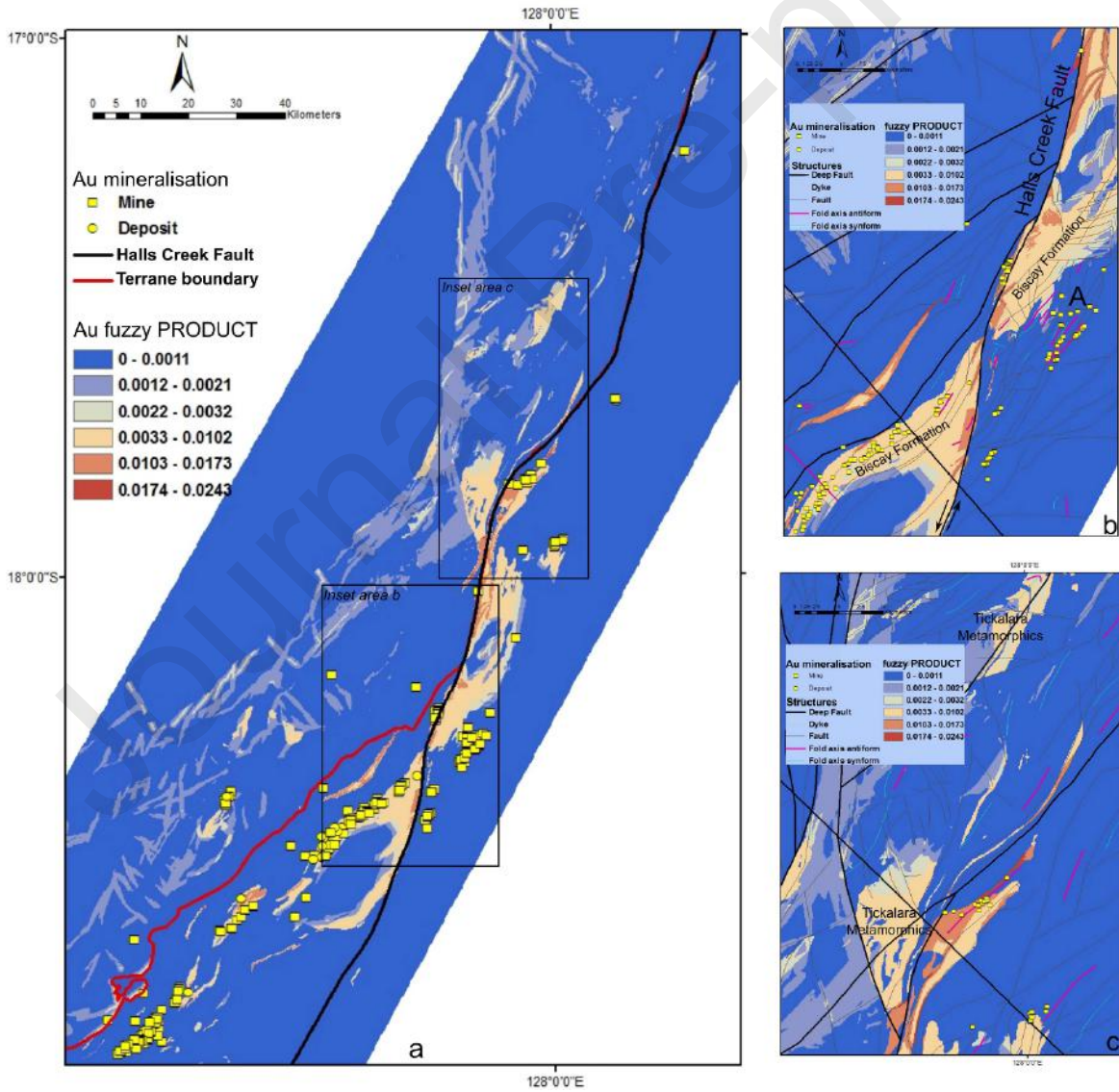
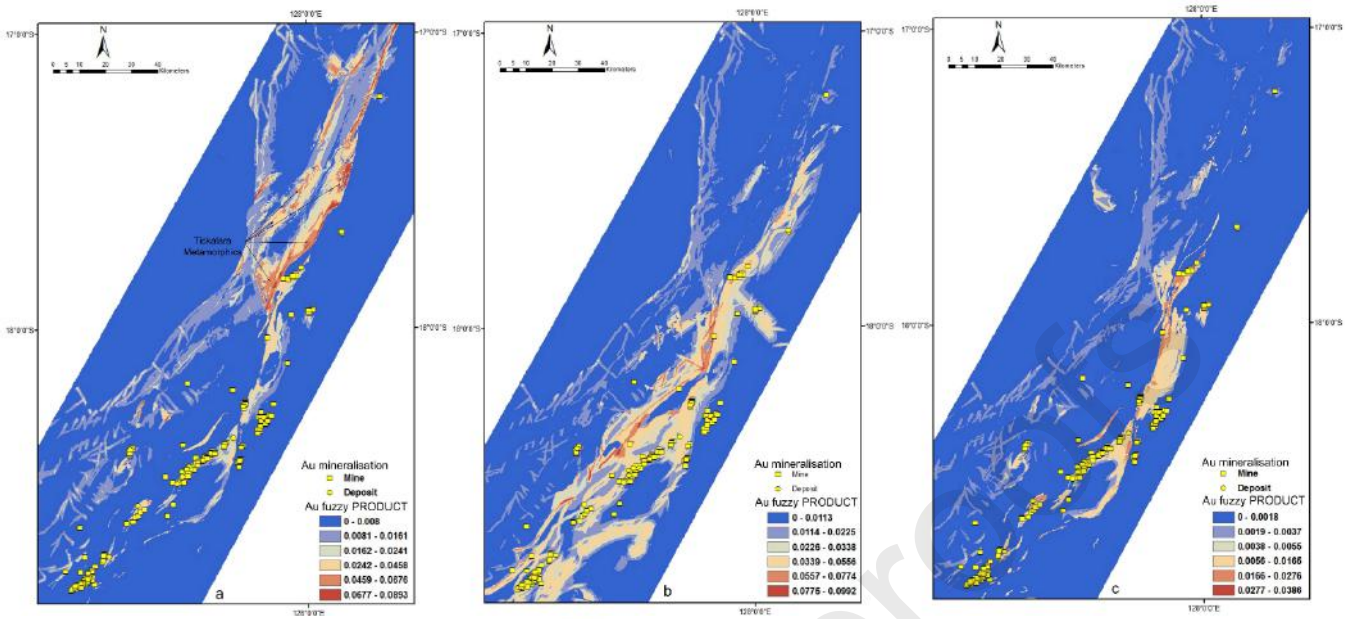
| <i>Mineral systems</i> | <i>Percentage of map in the top 50th percentile of map (Prospective)</i> | <i>Area (km²)</i> |
|-------------------------|---|------------------------------|
| Orogenic gold deposit | 3.2 | 742 |
| Magmatic nickel sulfide | 2.2 | 517 |
| <i>Mineral systems</i> | <i>Percentage of map in the low 50th percentile of map (Unprospective)</i> | <i>Area (km²)</i> |
| Orogenic gold deposit | 96.8 | 22325 |
| Magmatic nickel sulfide | 97.8 | 22550 |

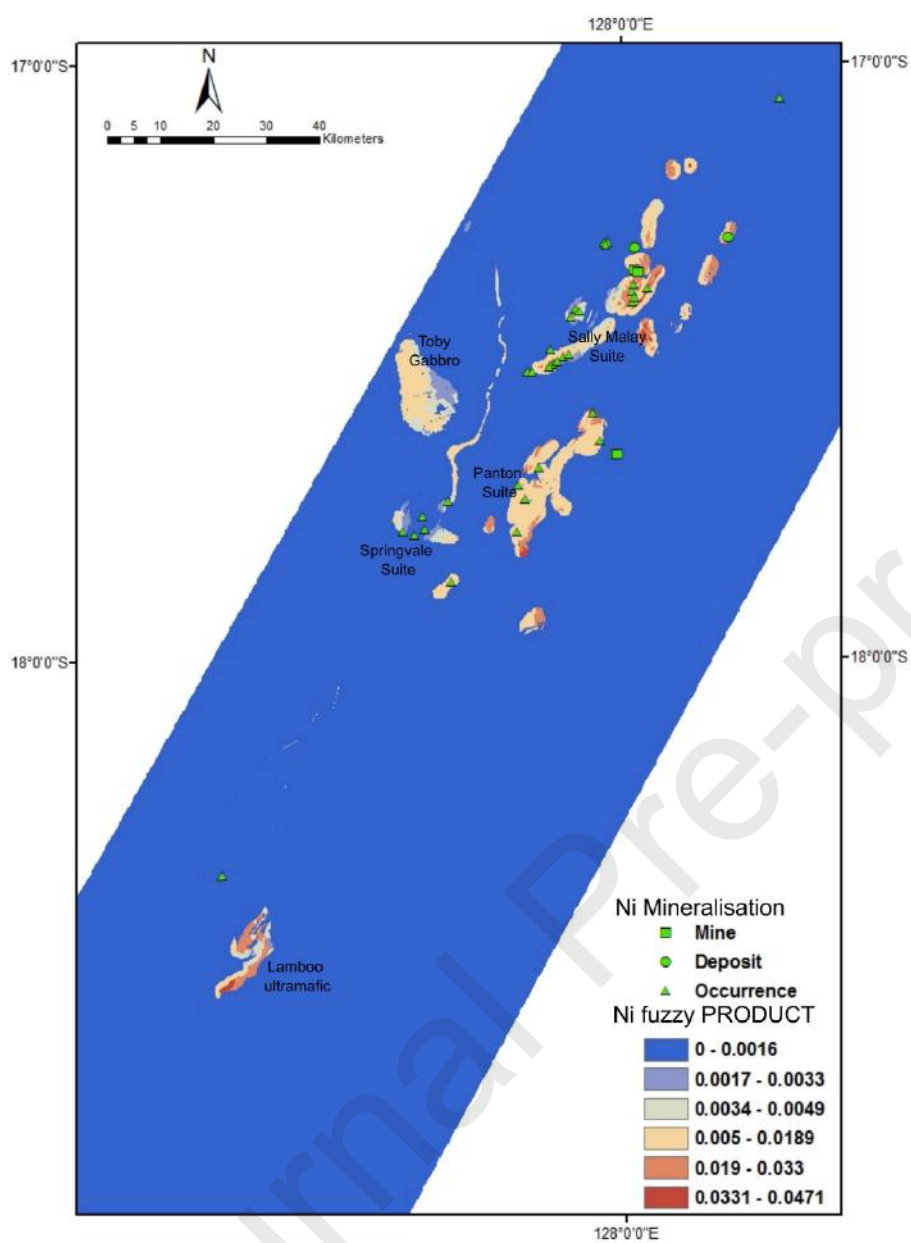
Table 5. Search area reduction statistics for orogenic gold deposit prospectivity models

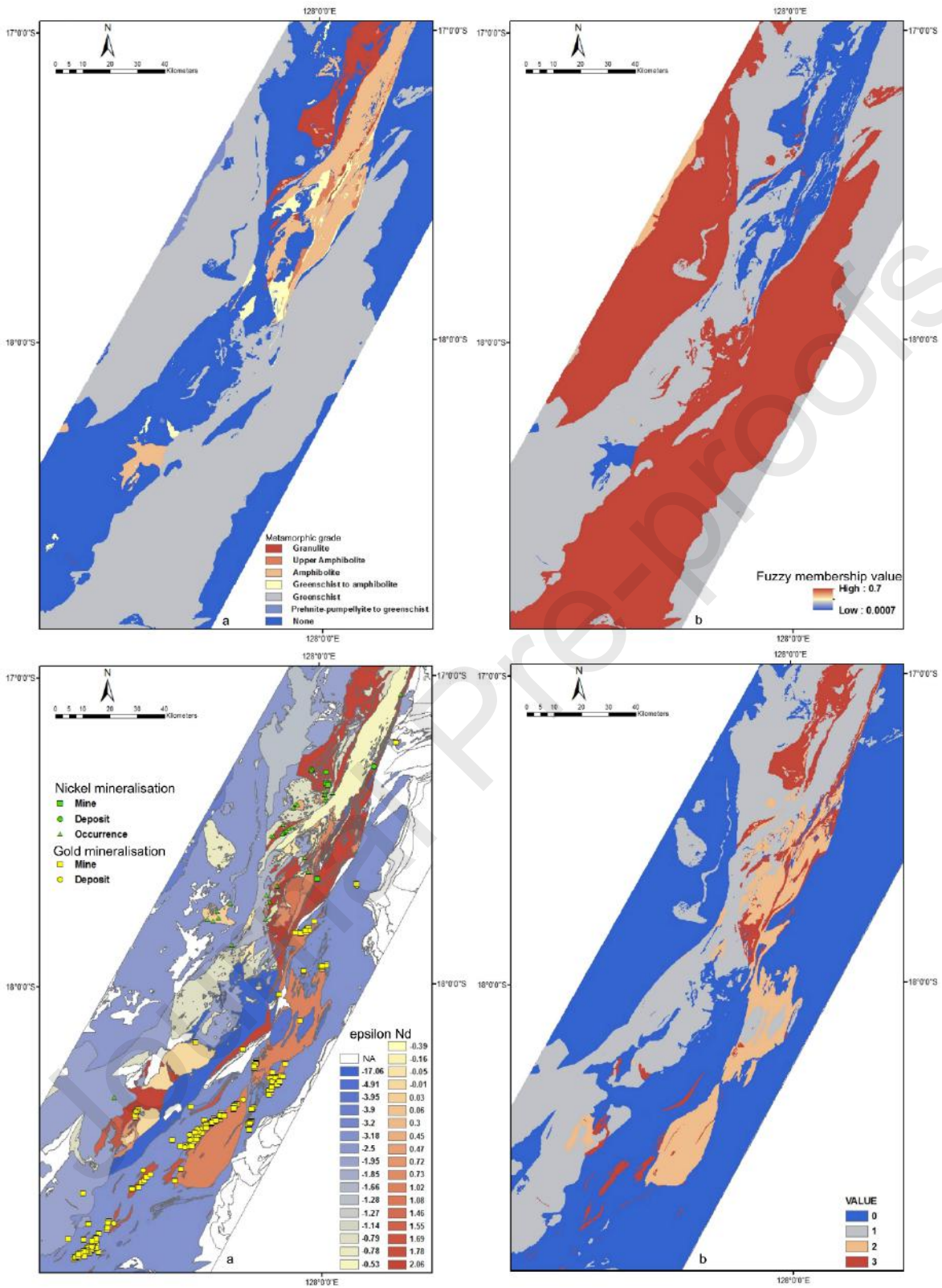
| <i>Models</i> | <i>Percentage of map in the top 50th percentile of map (Prospective)</i> | <i>Area (km²)</i> |
|--|---|------------------------------|
| Without preservation (metamorphic map) component (Fig.14a) | 4.13 | 952.7 |
| Without fertility (isotopic map) component (Fig.14b) | 6.86 | 1582.6 |
| Without source component (Fig. 14c) | 3.4 | 781.4 |
| <i>Models</i> | <i>Percentage of map in the low 50th percentile of map (Unprospective)</i> | <i>Area (km²)</i> |
| Without preservation(metamorphic map) component (Fig.14a) | 95.87 | 22114.3 |
| Without fertility (isotopic map) component (Fig.14b) | 93.14 | 21484.4 |
| Without source component (Fig. 14c) | 96.6 | 22285.6 |

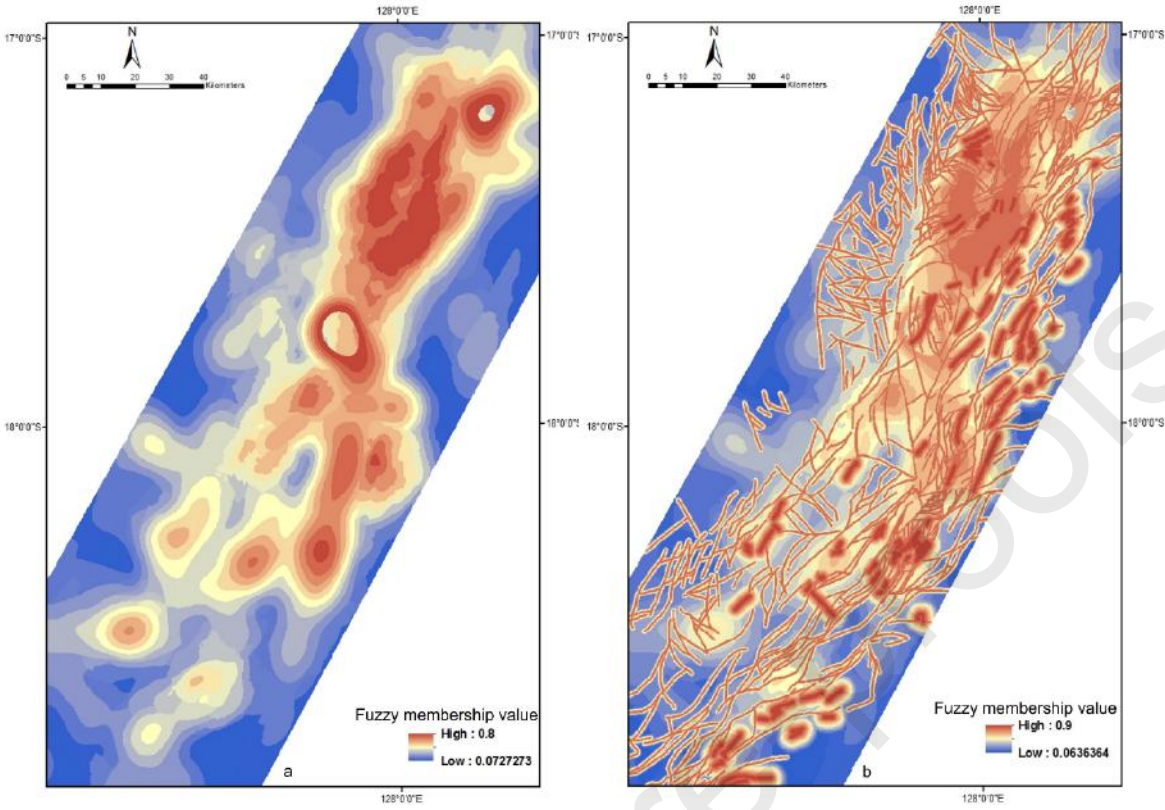
Highlights:

- ✓ The link between nickel and gold mineral systems in the Halls Creek Orogen (HCO).
- ✓ Mineral systems analysis by integration of geodynamics, geophysics and isotopes.
- ✓ Strong association between nickel–gold mineralisation and positive ϵNd value.
- ✓ Whole-rock Nd confirmed the input of juvenile melts in the centre of the HCO.
- ✓ $^{40}\text{Ar}/^{39}\text{Ar}$ revealed the relation of gold mineralisation and basin closure.









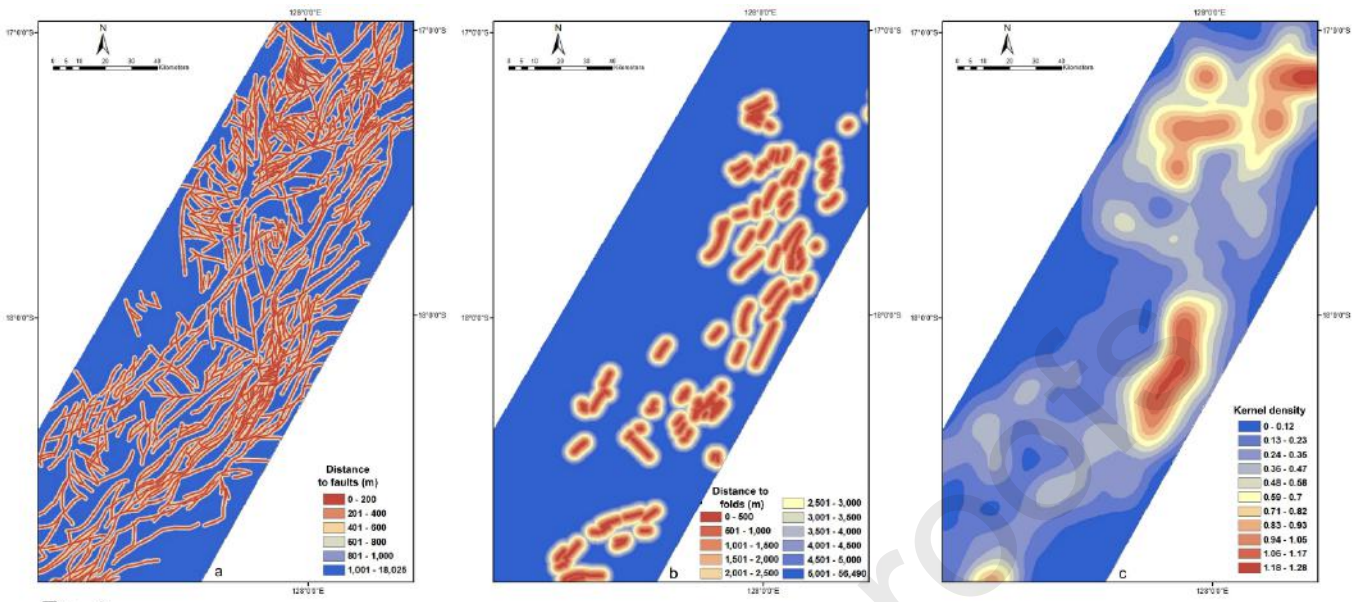
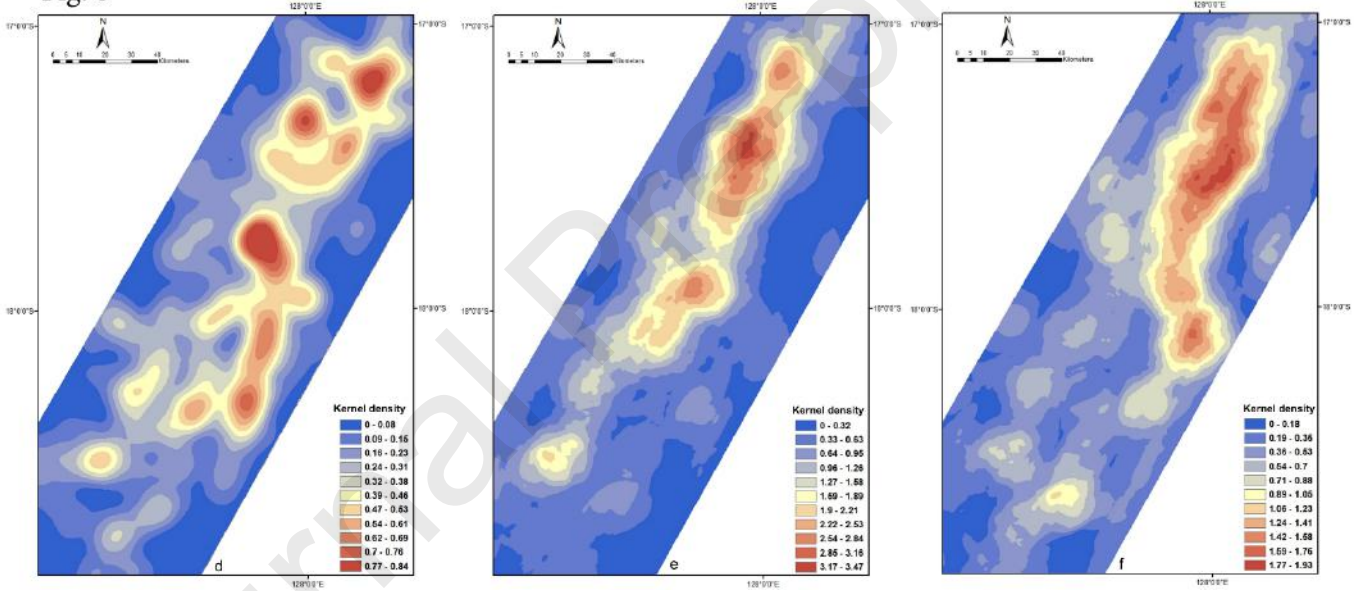
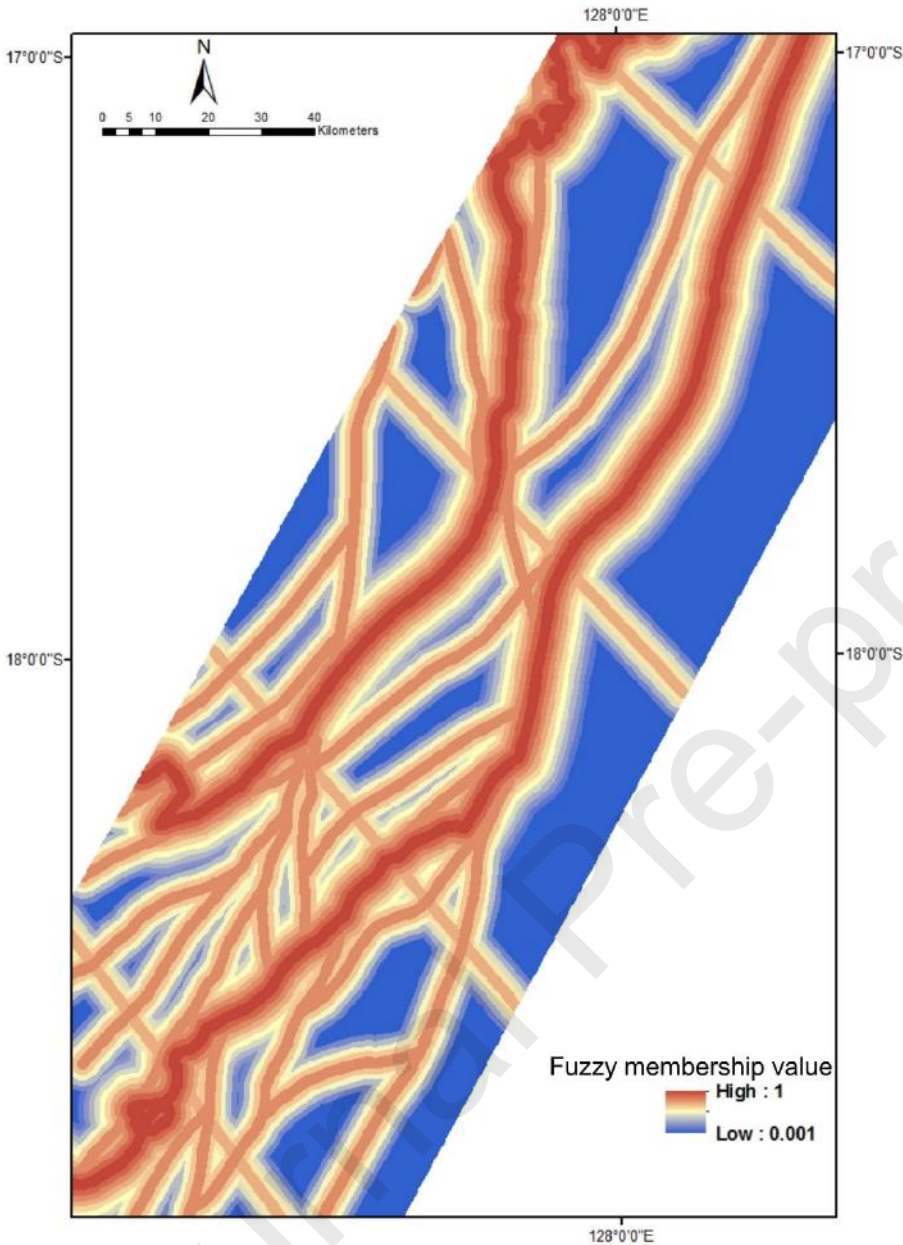
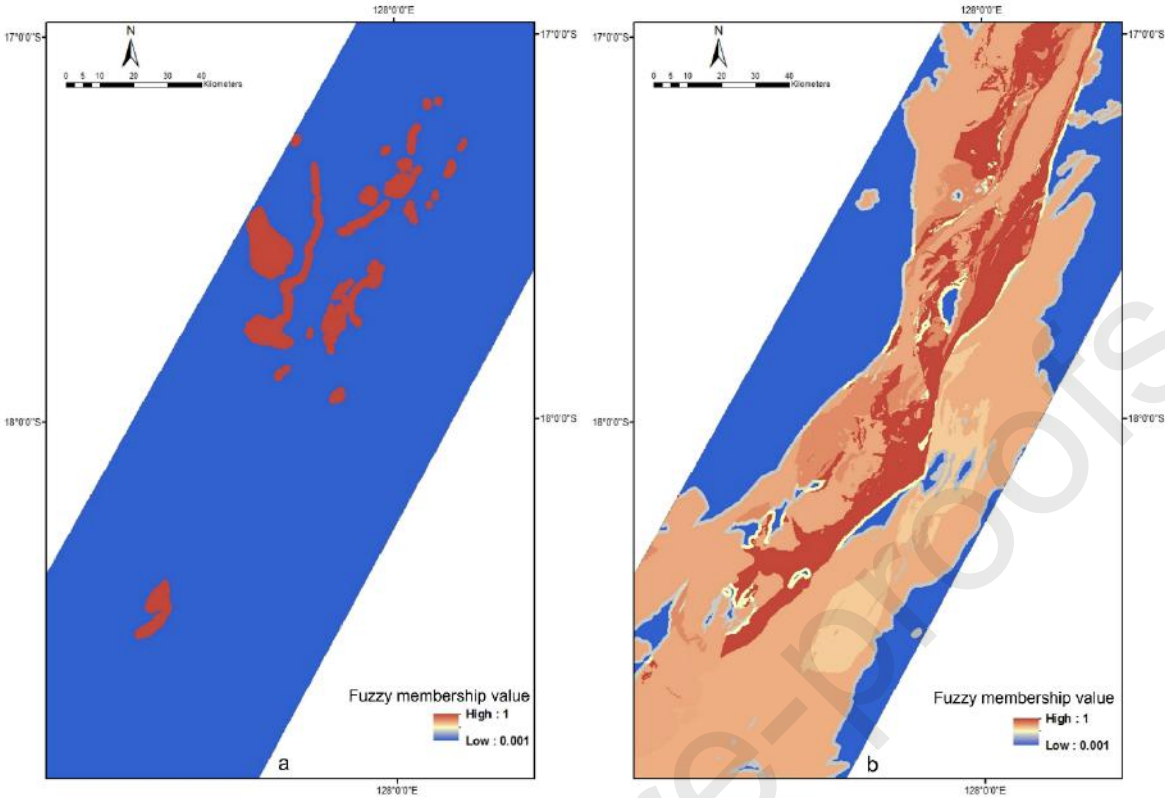
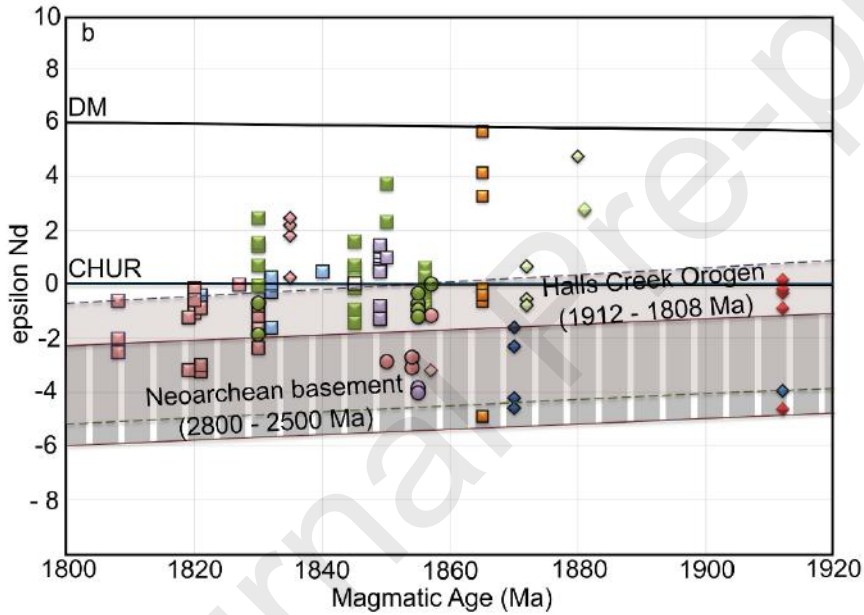
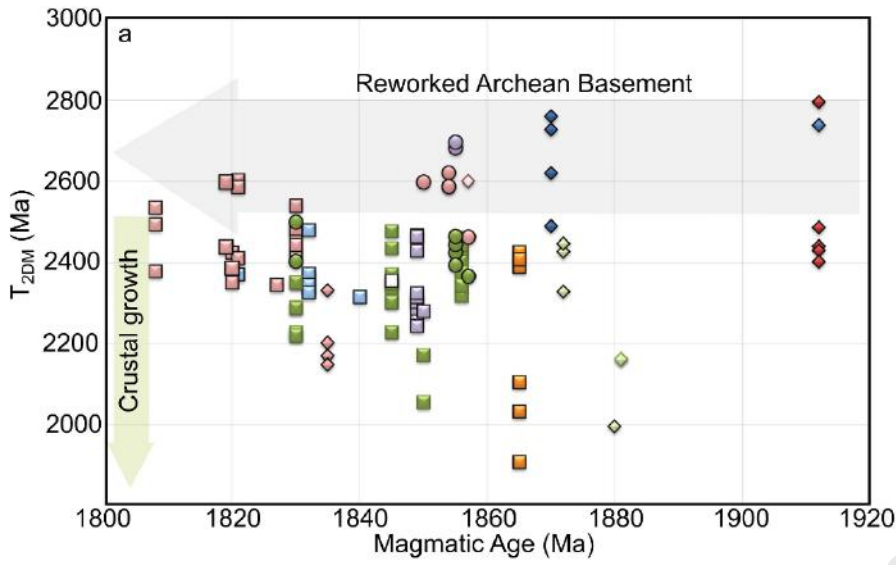


Fig. 8

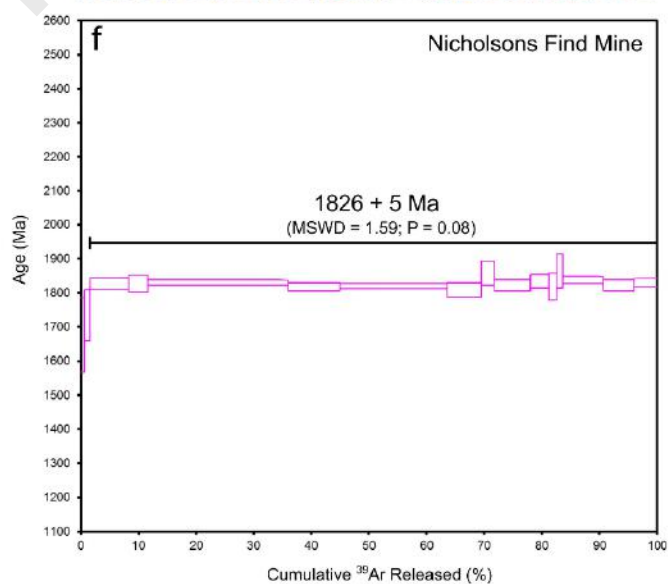
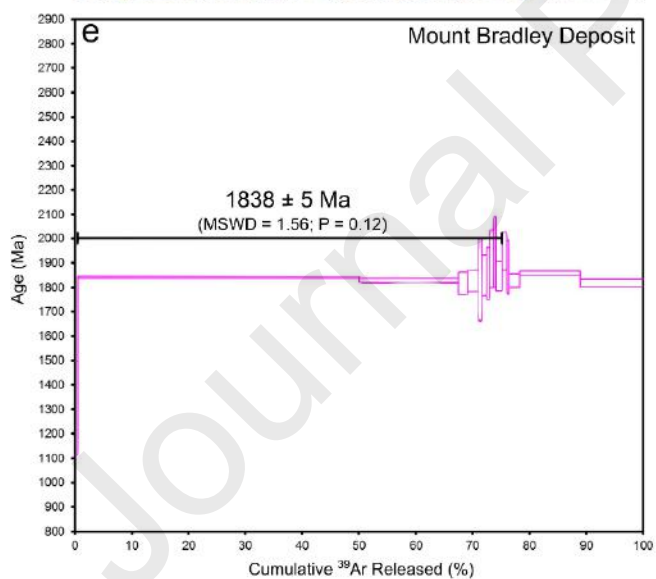
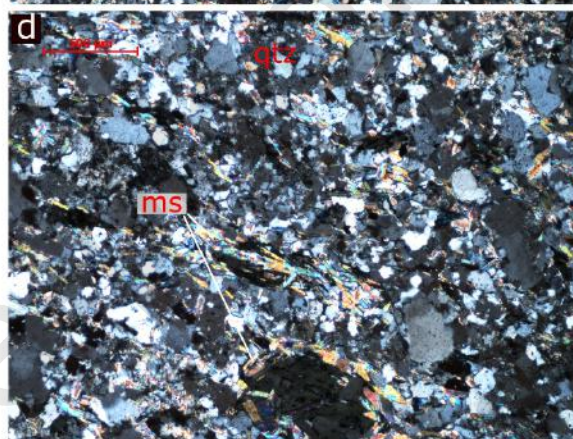
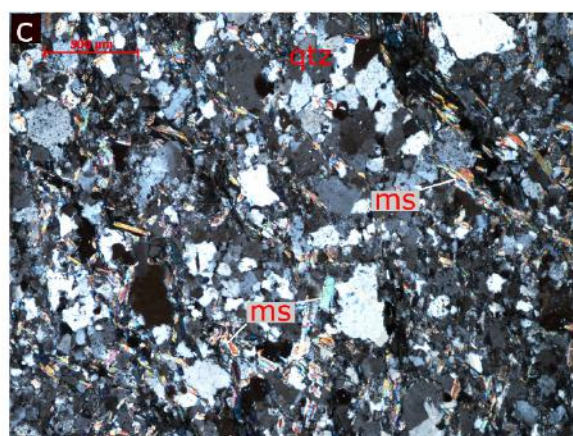
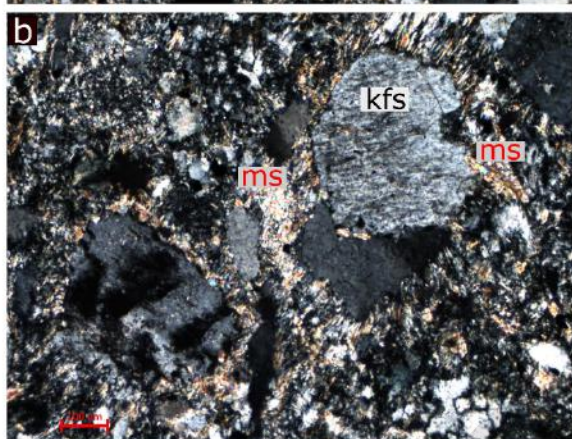
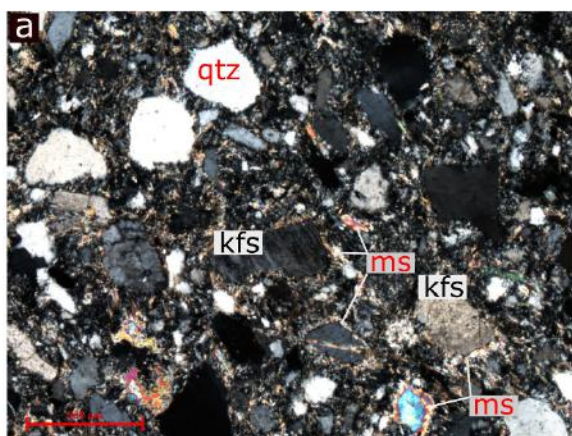


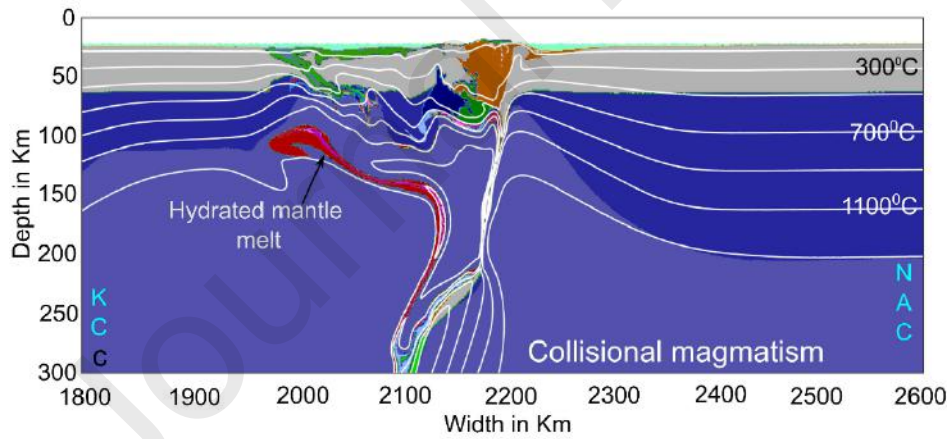
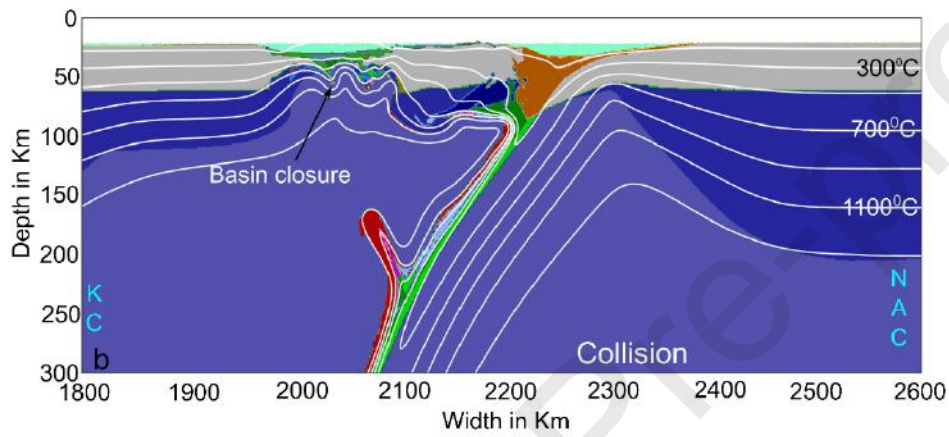
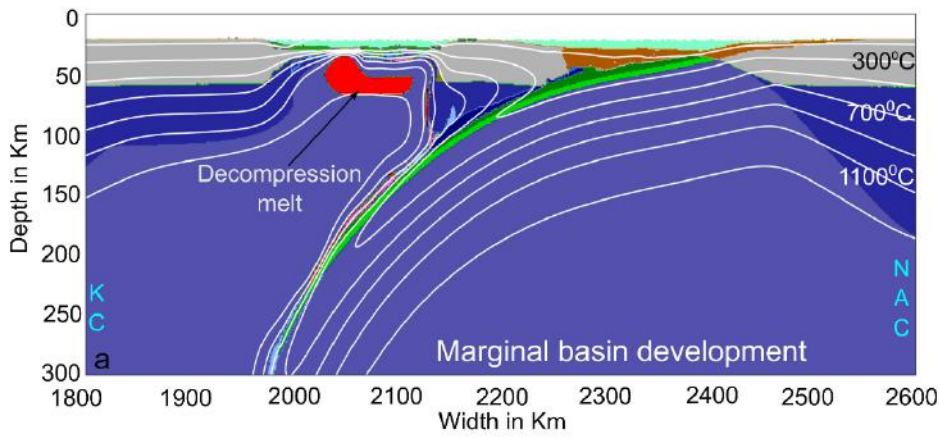




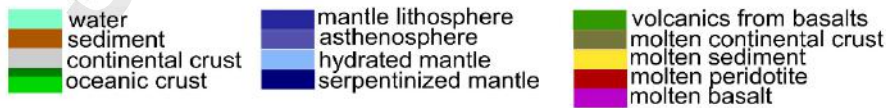


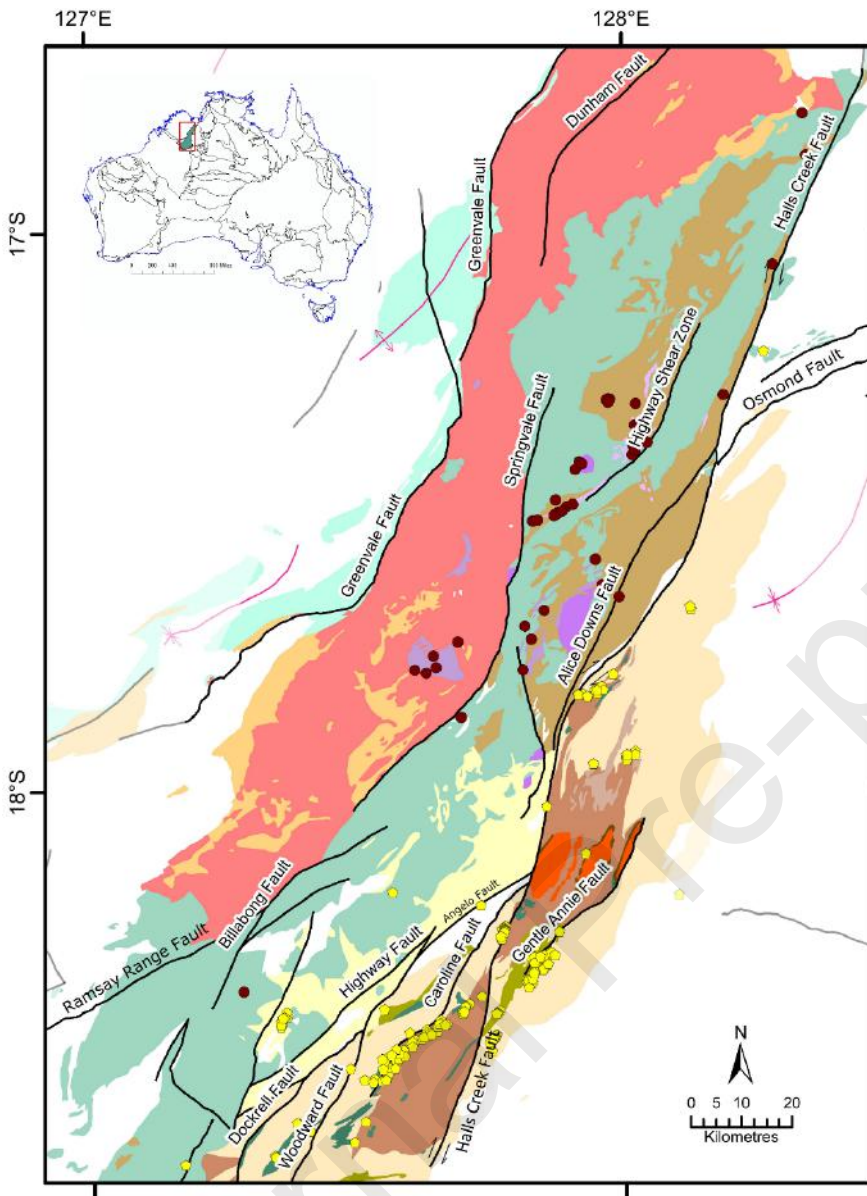
- | | | |
|-----------------------------|--------------------------|--------------------------|
| ◇ Eastern Zone | □ Central Zone | ○ Western Zone |
| ◆ Sophie Downs Granite | ▣ Tickalara Metamorphics | ● Paperbark Supersuite |
| ◆ Ding Dong Downs Volcanics | □ Koongie Park Formation | ● Whitewater Volcanics |
| ◇ Biscay Formation | ▣ Dougalls Suite | ● Mafic-Ultramafic units |
| ◇ Brim Rockhole Formation | ▣ Mafic-Ultramafic units | |
| ◆ Olympio Formation | ▣ Mable Downs Suite | |
| ◇ Maude Headley Member | ▣ Sally Downs Supersuite | |
| ◆ Woodwrd Dolerite | | |





Rock type or melt:





Legend

WESTERN ZONE

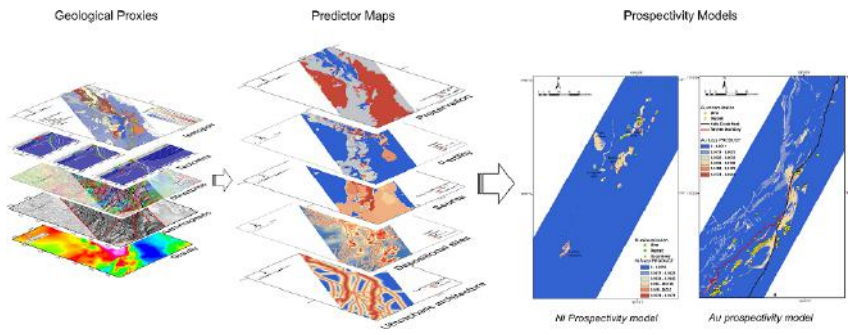
- Whitewater Volcanics
- Springvale Suite
- Paperbark Supersuite
- Marboo Formation
- Nickel occurrences
- Gold deposit

CENTRAL ZONE

- Sally Downs Supersuite
- McIntosh, Armanda, and Spring Creek intrusions
- Koongie Park Formation
- Sally Malay intrusions
- Panton Intrusions
- Tickalara Metamorphics

EASTERN ZONE

- Woodward Dolerite
- Olympio Formation
- Butchers Gully Member
- Maude Headley Member
- Biscay Formation
- Saunders Creek Formation
- c. 1910 Ma basement



Journal Pre-proofs